Title

Rapid manifestation of reactive astrogliosis in acute hippocampal brain slices

Permalink

https://escholarship.org/uc/item/4hm682h6

Journal

Glia, 62(1)

ISSN

0894-1491

Authors

Takano, Takahiro
He, Wei
Han, Xiaoning
et al.

Publication Date

2014

DOI

10.1002/glia.22588

Peer reviewed

Rapid manifestation of reactive astrogliosis in acute hippocampal brain slices

Takahiro Takano[1,3], **Wei He**[1,3], **Xiaoning Han**[1,3], **Fushun Wang**[1], **Qiwu Xu**[1], **Xiaohai Wang**[1], **Nancy Ann Oberheim Bush**[1], **Nancy Cruz**[2], **Gerald A. Dienel**[2], and **Maiken Nedergaard**[1]

[1]Division of Glial Disease and Therapeutics, Center for Translational Neuromedicine, University of Rochester Medical Center, Rochester, New York 14642

[2]Dept. of Neurology, University of Arkansas for Medical Sciences, Little Rock, AR 72205

Abstract

A flurry of studies over the past decade has shown that astrocytes play a more active role in neural function than previously recognized. Hippocampal slices prepared from young rodent pups have served as a popular model for studying the pathways by which astrocytes participate in synaptic transmission. It is, however, not known how well astrocytes tolerate traumatic injury and hypoxia, which are unavoidable when preparing acute slices. We here show that astrocytes exhibit striking changes in expression of several receptors and structural proteins, including re-expression of the developmental marker nestin within 90 min following preparation of live vibratome slices. Moreover, immunoelectron microscopy showed a 2.7-fold loss of astrocytic processes in acute hippocampal slices prepared from GFAP-GFP reporter mice. A sharp decrease in the number of mitochondria was also noted in acute slices, concurrently with an increase in mitochondrial size. Glycogen content decreased 3-fold upon slice preparation and did not recover despite stable recordings of field EPSC. Analysis of Ca^{2+} signaling showed that astrocytic responses to purine receptor and mGluR5 agonists differed in slice vs. *in vivo*. These observations suggest that the functional properties and the fine structure of astrocytes in slices may be reflective of early stages of reactive gliosis and should be confirmed *in vivo* when possible.

Keywords

Astrocytes; Interstitial space; NADH, Two-photon microscopy; Mitochondria; Electron microscopy; Purinergic receptors

Introduction

The first electrical recording in an acute brain slice preparation was published more than 40 years ago (Yamamoto and McIlwain 1966). Shortly thereafter, hippocampal slices quickly

gained popularity as tools for the study of long-term potentiation (LTP) (Brown et al. 1988; Schwartzkroin and Wester 1975; Skrede and Westgaard 1971). The ability to obtain stable intracellular recordings for prolonged periods with sharp electrodes added to the popularity of slice preparation (Sarvey et al. 1989). The patch clamp technique developed by Sakmann and Neher (Neher and Sakmann 1976; Sigworth and Neher 1980) in membrane patches of denervated frog muscle fibers was initially adapted to cultured hippocampal slices (Llano et al. 1988) followed by acute slices (Edwards et al. 1989). Most analysis of circuit function and synaptic plasticity is now based on patch clamp using differential interference contrast (DIC) optics and infrared light for guidance (Dodt and Zieglgansberger 1990).

While it has been documented that key neuronal functions are largely preserved in slices, it is also acknowledged that microglial cells exhibit rapid activation following exposure to acute trauma or hypoxia (Kettenmann et al. 2011). Additionally, GFAP staining of fine astrocytic processes is diminished in slices fixed after 4 h incubation *in vitro* compared with fixation immediately after slicing, whereas neuronal S100β and MAP2 staining remains relatively unaffected (Ball et al. 2007). However, little information exists with regard to how well astrocytes tolerate slice preparation and how quickly changes take place thereafter. Astrocytes are the principal supportive cells of the brain and several of their functions, including K^+ buffering and glutamate uptake, are critical for synaptic transmission (Allen and Barres 2009; Nedergaard and Verkhratsky 2012). During slice preparation, astrocytes are faced with an "environmental disaster", which includes >5–15 min anoxia, energy failure, traumatic injury inflicted by the vibratome, and exposure to cytosolic and blood born components; in fact, since the pioneering studies of McIlwain and colleagues, the 'health' of brain slices, effects of preparative methods, and other factors that influence experimental outcome in slices have been long-standing issues (Aitken et al. 1995; Langmoen and Anderson 1981; Lipton et al. 1995). Furthermore, it is routine during the cutting of vibratome slices to immerse the brain in a "cutting solution", in which Na^+ is exchanged with sucrose or N-methyl-d-glucamine (NMDG). This approach reduces excitatory injury of CA3 pyramidal neurons, but may add additional stress on astrocytes, which are sensitive to changes in interstitial ion concentration and osmolarity (Kimelberg 2007; Nedergaard and Verkhratsky 2012).

Studies in live animals have shown that reactive changes of astrocytes coincide with the re-expression of intermediate filaments, such as nestin, as early as 1 to 8 h after traumatic injury (Kaneko et al. 2012). Such rapid changes in astrocytic gene expression occur within the timeframe where recordings in hippocampal slices are considered optimal (Edwards et al. 1989). To directly assess the impact of slice preparations on astrocytic morphology and protein expression, we have here assessed changes in the ultrastructure of astrocytes, as well as expression of selected structural proteins and receptors, after incubation of hippocampal slices in oxygenated artificial cerebrospinal fluid (aCSF) for 1–3 h. Our data suggest that shortly after slice preparation, astrocytes retract their fine processes and exhibit reactive changes that are consistent with the early stages of reactive astrocytosis. Thus, astrocytes in acute hippocampal slices differ from those in live animals, both structurally and with regard to expression of structural proteins and receptors.

Materials and Methods

Slice preparation and field excitatory postsynaptic current (fEPSC) recordings

14–17 day old FVB/NJ mice were used for preparation of cortical or hippocampal slices as previously described (et al. 2003; Kang et al. 1998; Torres et al. 2012). The pups were anesthetized in a closed chamber with isofluorane (1.5%) and decapitated. The brains were rapidly removed and immersed in ice-cold cutting solution that contained (in mM): 230 sucrose, 2.5 KCl, 0.5 $CaCl_2$, 10 $MgCl_2$, 26 $NaHCO_3$, 1.25 NaH_2PO_4, and 10 glucose, pH=7.2–7.4. Coronal slices (400 μm) were cut using a vibratome and transferred to oxygenated aCSF that contained (in mM): 126 NaCl, 4 KCl, 2 $CaCl_2$, 1 $MgCl_2$, 26 $NaHCO_3$, 1.25 NaH_2PO_4, and 10 glucose, pH = 7.2–7.4, osmolarity 310 mOsm. The slices were placed in a chamber at the microscope stage and superfused with aCSF gassed with 5% CO_2 and 95% O_2 at room temperature. EPSCs were evoked using a single 0.10 ms biphasic pulse delivered through a constant isolated current source (IsoFlex Isolator, and Master-8, AMPI, Israel) and applied to the Schaffer collaterals using a concentric platinum/ iridium bipolar electrode (CBARC75, FHC, Brunswick, ME), and recorded with a pipette filled with aCSF or saline positioned in the CA1 region. EPSCs were recorded by an amplifier (700B, Axon Instruments Inc.), and the pCLAMP 10.1 program and DigiData 1440 interface (Molecular Devices) with an interval of 20 μs. Stimulation was adjusted to evoke 60% of the intensity necessary to evoke a maximum EPSC response as determined from input/output curve construction. Individual EPSCs were evoked and recorded every 60 s and recorded continuously for 2 h.

Animal preparation for *in vivo* 2-photon imaging

14–17 day-old mouse pups of either sex were anesthetized with an i.p. injection of ketamine (0.12 mg g^{-1}) and xylazine (0.01 mg g^{-1}). Depth of anesthesia was monitored by pinch withdrawal and anesthesia was supplemented with half the initial dose of ketamine and xylazine every hour or sooner if the mice responded to pinch stimulation. Body temperature was maintained at 37°C by a heating blanket. A craniotomy (2–3 mm in diameter), centered 0.5 mm posterior to the bregma and 3.5 mm lateral from midline, was made over the right primary somatosensory cortex, and the dura was removed. A custom-made metal plate was glued to the skull with dental acrylic cement. For Ca^{2+} imaging, rhod-2 AM (10 μM, Life Technologies) was dissolved in dimethyl sulfoxide with 20% pluronic acid and mixed in aCSF. After 15–25-min loading, the exposed brain was washed for 15 min with aCSF without dye. No dye was used in *in vivo* NADH imaging. Agarose (1%, 37 °C) was poured on the cranial window and the glass cover slip was glued to the metal plate with dental acrylic cement. All experiments were approved by the Institution Animal Care and Use Committee of the University of Rochester.

In vivo and *ex vivo* two-photon imaging for quantification of agonist-induced intracellular Ca^{2+} concentration

A custom-built microscope attached to Tsunami/Millennia laser (Spectra Physics), a scanning box (modified from Olympus FV300) using FluoView software (Olympus), and a 20× objective (0.95 NA, Olympus) was used for two-photon imaging. Slices were incubated in aCSF for 1 hour at room temperature before 15–25 min loading with rhod-2 AM (5 μM).

Experiments were performed at room temperature (21–24 °C). Astrocytic Ca^{2+} concentration changes were induced by puffing of aCSF containing the agonists at a depth of ~100 μm below the surface in cortical and hippocampal slices or ~100 below the pial surface (cortical layer II – III) in live imaging experiments. The micropipettes where filed with aCSF containing Alexa Fluor 488 (100μM, Life Technologies) to visualize agonist delivery using picospritzer III (50 msec duration, 10 psi). Agonists included 3,5-dihydroxyphenylglycine (DHPG, 200μM, Tocris), (±)-1-aminocyclopentane-*trans*-1,3-dicarboxylic acid (tACPD, 500μM, Tocris), and adenosine triphosphate (ATP, 500μM, Sigma). Excitation wavelength was in the range of 820–840 nm. Two-channel detection of emission wavelength was achieved by using a 565-nm dichroic mirror and two external photomultiplier tubes. A 620/60 bandpass filter was used to detect rhod-2 AM emission wavelength. Time-lapse images of astrocytic Ca^{2+} signaling were recorded every 1 s. Percentage of responding cells was quantified by counting the number of cells that displayed increases of intracellular $[Ca^{2+}]$ (rhod-2 emission signal) higher than two standard deviations above baseline in response to agonist application. The baseline was measured as the mean intensity of frames preceding the application of agonist. Signal intensity was calculated in individual cells by measurement of rhod-2 signal using a circular region of interest in ImageJ software (NIH). On average, 25–50 cells per mouse were assessed.

In vivo and *ex vivo* two-photon imaging for NADH intrinsic fluorescence

NADH *in vivo* imaging was carried out as previously described (Takano et al. 2007). Briefly, a cranial window was prepared and 1% FITC-dextran was administered i. v. to visualize the cerebral vasculature in animals anesthetized with 1% isofluorane. The animals were placed under the 2-photon microscope. NADH was imaged at 740 nm using two-photon excitation and emission filtered with BGG22 colored glass (Schott) or a 460/40 nm bandpass filter. 0.1 M KCl solution was topically applied to the open cranial window while a series of images were captured at 3 s intervals in cortical layer I. The perivascular regions were defined as the 25 μm radius from the center of penetrating arteries, which were identified by both bright field and FITC-dextran fluorescence. Using a similar method, NADH slice imaging was collected before and 1, 3, and 6 min after 0.1 M KCl solution was applied to a perfusion chamber containing acutely-isolated slices in oxygenated aCSF. On selected experiments, astrocytes were identified using transgenic mice that express GFP under a promoter for the glutamate transporter GLT-1 (Regan et al. 2007). Selected slices were stained for mitochondria with rhodamine 123 (10 μM for 10 min, Life Technologies). Rhodamine 123 or GFP was imaged with 515/50 nm emission filter. Average NADH fluorescence intensity was measured with Image J software and percent intensity of the initial image before KCl application was calculated.

Iontophoretic tetramethylammonium (TMA) quantification of the interstitial space volume

Vibratome sections (400 μm thick) were prepared as described above and transferred to the microscope stage after 1 h incubation in oxygenated aCSF. The single-barrel iontophoresis microelectrode contained 150 mM TMA-chloride (World Precision Instruments TW150-4, 3 μm tip diameter). For measurements of TMA, microelectrodes with an outer diameter of 2–4 μm were fabricated from double-barreled theta-glass (World Precision Instruments PB150F-4, 3 μm tip diameter) using a tetraphenylborate-based ion exchanger (Corning

477317, World Precision Instruments). The TMA barrel was backfilled with 150mM TMA-chloride, whereas the reference barrel contained 150 mM NaCl. The TMA signal was calculated by subtracting the voltage measured by the reference barrel from the voltage measured by the ion-detecting barrel, using a dual-channel microelectrode preamplifier (model IX2–700; Dagan). The Nikolsky equation was used for calibration of the TMA electrodes based on measurements obtained in oxygenated aCSF containing 0.5, 1, 2, 4, and 8 mM TMA-chloride in 150 mM NaCl (Nicholson 1992; Nicholson et al. 2011; Sykova and Nicholson 2008).

Immunohistochemistry, image analysis, and data processing

Littermates of 14–17-day-old FVB/NJ mouse pups of either sex were used for the immunohistochemical analysis. Littermates were divided into groups that were either perfusion-fixed with 4% paraformaldehyde or immersion-fixed in 4% paraformaldehyde following 0 or 90 min incubation of the 400-μm live vibratome sections in oxygenated aCSF at room temperature. Following overnight fixation, the sections were embedded in 6% agarose and sagittal sections with a thickness of 50 μm were generated from the 400-μm sections using vibratome sectioning (Fig. 1A). The sections were individually placed in 24-well culture dishes and washed several times in 0.1 M PBS. The sections were permeabilized and blocked with a solution of 1% L-lysine monohydrochloride (Sigma) in 0.1 M PBS and 100 μl Triton X-100 (0.1%) for 24 h at 4°C. Tissue sections were then incubated in a solution of primary antibody diluted in the permeabilizing–blocking agent for a period of 72 h. The antibodies included a GFAP monoclonal antibody (G3893, 1:100; Sigma), a chicken polyclonal antibody against MAP2 (ab5392, 1:100, Abcam), a polyclonal antibody against nestin (PRB-315C, 1:100, Covance), a polyclonal antibody against aquaporin 4 (AQP-4) (AB3068, 1:100; Chemicon International, Temecula, CA); a polyclonal antibody against Cx43 (71–0700, 1:500; Zymed Laboratories, San Francisco, CA), polyclonal antibodies against P2YR2 and P2YR4 (APR010 and APR006, 1:50 for both antibodies; Alomone Labs, Jerusalem, Israel), or a polyclonal antibody against mGluR5 (1:300, Upstate Biotechnology, Lake Placid, NY). After several washes in PBS, the sections were incubated with Cy2-, Cy3-, or Cy5-conjugated secondary antibodies (1:100, Jackson Laboratories) in PBS containing 1% donkey serum and 0.3% Triton X-100 at room temperature for 2 h. The reactions were completed by washing PBS several times and the sections were mounted with Prolong Antifade Gold with DAPI (Life Technologies). Immunofluorescence was visualized using a Bio-Rad MRC500 confocal scanning microscope attached to an inverted microscope (IX81, Olympus, Tokyo, Japan) with a 20× oil-immersion objective (NA 0.80). Stacks of images were collected with a 1 μm step for each field, and the projection image of the stack was used for the quantification. The parameters for confocal image capture (laser, power, photomultiplier tube voltage, gain, and offset) were first set from control staining with omission of primary antibodies and remained constant for collection of images from perfusion-fixed and immersion-fixed slices for each combination of antibody staining. The intensities of the antibody labeling in the 3 groups (perfusion-fixed, immersion-fixed at 0 and 90 min) were compared by first averaging the intensities of the labeling across the entire z-sections for each slice, then the averaged values (% control) were normalized to that of the perfusion-fixed control. The correlation of the distance from the slice surface across the 400 μm thick section with the intensity of

immunolabeling at each depth were plotted by first sequentially measuring the labeling intensities in a 10 μm × 10 μm field each, from one surface to the other surface (~40 fields across the section), then in each slice the intensity of each 10 × 10 field was normalized to the overall average of the all fields combined in the perfusion-fixed slice.

Diolistic labeling

The Helios Gene Gun System (165–2431; Bio-Rad, Hercules, CA) was used to deliver gold (1.0 μm) coated with lipophilic dyes into perfusion- or immersion-fixed brain slices (4% paraformaldehyde) as previously described (Oberheim et al. 2008). Briefly, 2–4 mg of DiI (D282; Life Technologies) was dissolved in 200 μl of methylene chloride (Sigma) and added to 0.05 g of gold or tungsten, dried, then dissolved in 3 ml of double-distilled H_2O. The solution was drawn into Tefzel tubing using a syringe and rotated three to four times. The water was slowly drawn out of the tube using a syringe, and the tube was allowed to air dry for 5 min before cutting into bullets using the tube cutter. The brain slices (400 μm thick) were placed on 2% agarose blocks in a culture dish and shot with both DiI bullets using 100 psi of helium pressure. Slices were counterstained with Sytox (Life Technologies) and mounted for confocal imaging.

Tissue preparation, processing, and quantification of electron microscopic studies

A total of 9 postnatal 14–17d GFAP-GFP pups and 9 adult postnatal 55–66d GFAP-GFP mice (Zhuo et al. 1997) were used for immuno electron microscopic (EM) studies. For preparation of control immunoEM, the animals were perfusion-fixed with a mixture of 4% paraformaldehyde and 0.1% glutaraldehyde fixative in 0.1 M phosphate buffer (pH 7.4). Their brains were removed from the skulls, post-fixed in 4% paraformaldehyde for 24 hours, sectioned in 50 μm-thick coronal sections with a vibrating microtome (Vibratome 1000), and serially collected in phosphate buffer saline (PBS). The free-floating sections were washed overnight in PBS, incubated in 5% goat serum in PBS at 4°C for 1 h, and then incubated in rabbit anti-GFP (Life Technologies, 1:300) at 4°C overnight. After several washes in PBS, the slices were incubated with goat anti-rabbit (1:200, ABC Peroxidase Staining Kit, Pierce), washed in PBS, incubated with ABC reagent at room temperature for 1 h, and antibody binding was visualized with 0.025% 3, 3'-diaminobenzidine 0.003% H_2O_2 (Lovatt et al. 2007). In parallel, live 400-μm thick vibratome slices prepared from littermates were incubated for 0, 1, or 3 h in oxygenated aCSF followed by immersion-fixation in the 4% paraformaldehyde and 0.1% glutaraldehyde fixative. Following overnight fixation, 50 μm vibratome cross-sections were prepared from the immersion-fixed slices and immunoreacted against GFP in parallel with the sections prepared from the perfusion-fixed animals.

For regular EM, a total of 18 young pups (P14-P17 days) and 9 adult (55–66 days) FVB/NJ mice were fixed using a modified Karnovsky's solution containing 2% paraformaldehyde and 2% glutaraldehyde in 0.1 M phosphate buffer. Littermates were either perfusion-fixed or immersion-fixed following 0, 1, 3 h incubation of the 400-μm live coronal sections in oxygenated aCSF using the same fixative. After post-fixation for 24 hours, both the perfusion-fixed and immersion-fixed tissue was cut into 50 μm-thick sagittal sections which were incubated overnight in 0.1 M cacodylate buffer. Of note, only sections corresponding to a depth of 120–180 and 180–240 μm in the 400 μm sections were processed for regular

EM and immuno-EM. Stratum radiatum of CA1 region were isolated from the 50 μm sections under a dissecting microscope as 0.8mm × 0.8mm blocks. The blocks were post-fixed for 1 h in 1% osmium tetroxide (in 0.1 M cacodylate buffer, pH 7.4) at room temperature, dehydrated, embedded in Embed-812 (EMS, Washington, PA), polymerized at 60°C for 48 h, cut as ultra-thin sections (70 nm), and counter-stained with uranyl acetate and lead citrate.

From each of these blocks, 50 micrographs of randomly-selected images of approximately 36 μm^2 per field without cell bodies were taken at 26,000× using a Hitachi 7100 electron microscope (Tokyo, Japan). Up to six sections per animal were collected and included in the analysis. The interstitial space was defined as the area free of membranes or organelles in regular EM, whereas GFP$^+$ astrocytic processes were defined as the membrane-bound dark-stained cellular processes in immunoEM. The quantification of numbers and areas of interstitial space, GFP$^+$ or GFP$^-$ processes, and mitochondria were done blindly using ImageJ. The areas were normalized relative to the total area of the field, then the averages of 40 micrographs were obtained.

Glycogen and lactate measurements

Slices from 14–17-day-old mice were immediately frozen at the end of each incubation interval carried out at room temperature (21–24 °C), frozen slices were extracted with aqueous ethanol, and the insoluble pellets were washed. Lactate levels were assayed in the ethanol-soluble extracts, and glycogen contents of the ethanol-insoluble pellets were determined by difference, as net glucose released during parallel incubations in the presence and absence of amyloglucosidase (Cruz and Dienel 2002; Dienel et al. 2002).

Results

Astrocytes rapidly exhibit reactive changes in acute hippocampal slices

To evaluate how well astrocytes tolerate preparations of acute slices, we used routine procedures and cut 400 μm-thick hippocampal slices from 14–17 days old pups (Bekar et al. 2008; Kang et al. 1998; Sun et al. 2013). The slices were randomly divided into three groups that were either used for electrophysiology or immersion-fixed in 4% paraformaldehyde immediately after cutting (0 min) or following 90 min incubation in an oxygenated aCSF solution at 21–24°C. After overnight fixation, 100 μm × 400 μm cross-sections were prepared from the immersion-fixed slices. Similar sections were prepared in parallel, from littermates perfusion-fixed with 4% paraformaldehyde prior to harvesting their brains (Fig. 1A). To evaluate synaptic transmission in the hippocampal slices, we stimulated the Schaeffer's collateral and recorded field excitatory postsynaptic current (fEPSC) in the CA1 region (Fig. 1B). Recordings were obtained for periods of 2 h (1–3 h after vibratome cutting following a 1 h recovery period). The analysis showed that neuronal excitatory transmission, detected as fEPSC, remained stable with no decline in amplitude or duration during the 2 h recordings (Fig. 1C–D).

Upregulation of glial fibrillary acidic protein (GFAP) is a sensitive indicator of reactive changes in astrocytes and occurs at early stages in most brain pathologies (Verkhratsky et al.

2012). The intensity of GFAP immunolabeling was moderately, but significantly increased ($23.0\pm2.0\%$ $p<0.01$, Dunnett test) in hippocampal slices fixed at 90 min after preparation compared to slices immersion-fixed immediately (0 h) after vibratome cutting, or to slices prepared from perfusion-fixed littermates (Fig. 2A–B). Two sets of control slices were employed because the fixation (perfusion vs. immersion) may affect the protein conformation and thereby the affinity of the antibodies. The intensities of GFAP immunolabeling in the immersion-fixed slices (0 and 90 min) were normalized to the mean value the GFAP immunolabeling of perfusion-fixed slices prepared in parallel. In addition to comparing immunolabeling across these 3 groups, we also analyzed the intensity of GFAP labeling throughout slice immersion-fixed after 90 min incubation in oxygenated aCSF. In this analysis, the labeling intensity was normalized within each slice to best capture alterations in immunolabeling at the surface vs. the middle of the same slice. The analysis showed that the GFAP labeling was even throughout the thickness of the slices immersion-fixed at 90 min indicating that the increase in GFAP labeling occurred both in the middle and the surface of the slice that are regions of the slices expected to be more hypoxic and more damaged, respectively (*, $P < 0.05$, ANOVA with Tukey-Kramer test) (Fig. 2C). As expected, perfusion-fixed slices displayed an even labeling throughout the thickness of the slice.

Nestin is a type VI intermediate filament that is expressed by most dividing cells during the early stages of development in the CNS and other tissues. Upon differentiation, nestin is replaced by cell type-specific intermediate filaments, such as GFAP in astrocytes and neurofilament in neurons (Liem and Messing 2009). In control slices, only endothelial cells expressed nestin (Li and Chopp 1999) (Fig. 2D). However, essentially all astrocytes, in slices fixed after 90 min incubation in oxygenated aCSF at 21–24°C, were nestin positive (Fig. 2D–F). This observation is consistent with the prior reports indicating that nestin is rapidly re-expressed in response to traumatic brain injury or hypoxia *in vivo* (Clarke et al. 1994; Li and Chopp 1999).

Astrocytes are coupled by gap junctions composed primarily of connexin 43 (Cx43) (Dermietzel et al. 1989). Multiple studies have documented an increase in Cx43 expression after injury (Huang et al. 2012; Lin et al. 2008; Nakase et al. 2006; VanSlyke and Musil 2005). We here found that immunolabeling of Cx43 also exhibited a marked increase in slices incubated for 90 min in oxygenated aCSF ($127.1\pm3.4\%$ $p<0.01$, Dunnett test) (Fig. 2G–H). In most slices, the cell body and major processes of astrocytes were densely labeled with Cx43, instead of the punctate evenly-distributed pattern of Cx43 positive plaques observed in controls. Additionally, Cx43 labeling was more intense at the surface of the slices, possibly reflecting cellular injury inflicted by the vibratome cutting (Fig. 2I). Earlier studies have shown that Cx43 is rapidly upregulated after injury (Lin et al. 2008).

Aquaporin-4 (AQP4) is a water channel that is almost exclusively expressed by astrocytes in CNS (Lovatt et al. 2007; Nielsen et al. 1997). In the intact brain, the localization of AQP4 is highly polarized and more than 90% of AQP4 immunolabeling can be found in the vascular endfeet of astrocytes (Iliff et al. 2012; Mathiisen et al. 2010) (Fig. 2J). Interestingly, our analysis of acute vibratome slices revealed a striking redistribution of AQP4 immunolabeling. The stereotypical pattern of polarized expression of AQP4 in vascular

endfeet was partly lost, and the cell bodies and major processes of astrocytes became intensively labeled with anti-AQP4 antibodies (Fig. 2J–L).

Thus, all markers of reactive changes in astrocytes tested, i.e., GFAP, nestin, Cx43, and AQP4 were upregulated in acute slices. These observations indicate that astrocytes in hippocampal slices exhibit the classical signs of reactive gliosis at ~90 min, which is regarded as the optimal time for collection of electrophysiological recordings (Langmoen and Anderson 1981; Richard 1981)

Comparison of receptor expression and agonist-induced Ca^{2+} responses in acute slices and *in vivo*

Astrocytes are electrically non-excitable cells that signal by release of ATP and activation of purinergic receptors, including P2YR1, P2YR2, and P2YR4 (Cotrina et al. 1998; Guthrie et al. 1999). Purinergic receptors are characterized by rapid and prolonged desensitization (Franke et al. 2012; Tulapurkar et al. 2006). Because traumatic injury is associated with release of large amounts of cytosolic ATP (Abbracchio et al. 2009; Wang et al. 2004), we asked whether P2Y receptors are downregulated in hippocampal slices. We found that both P2YR2 and P2YR4 immunoreactivities were significantly reduced in slices fixed after 90 min compared with *in vivo* (Fig. 3A–F) (73.0±1.3% and 67.4±1.4% of control, respectively, p<0.01, Dunnett test). The expression of P2YR1 was not analyzed in this study, as the commercial antibodies that were tested labeled astrocytes in P2YR1 knockout mice. In contrast, the metabotropic glutamate receptor 5 (mGluR5) immunointensity exhibited a significant increase in acute hippocampal slices (Fig. 3G–H) (167.8±6.9% of control p<0.01, Dunnett test). The expression was relatively highest in the middle of the slices with relatively less immunostaining in tissue located just below the surface (Fig. 3I). The neuronal marker MAP2 exhibited a similar trend toward a general increase in immunolabeling intensity (116.4±3.0% of control, p<0.01, Dunnett test), but relatively lower immunoreactivity close to the surface of the slice, possibly reflecting neural injury (90.7±2.4% of overall intensity at the surface, p=0.0241, t test) (Fig. 3J–L).

We next asked whether the changes in receptor expression predict how astrocytes in hippocampal slices respond to agonist exposure. To directly compare agonist-induced Ca^{2+} signaling in acute slices vs. *in vivo*, acute slices were loaded with the fluorescent Ca^{2+} indicator, rhod-2 AM, and agonist-induced Ca^{2+} signaling was quantified using 2-photon excitation. In parallel, littermates were prepared for two-photon *in vivo* imaging as previously described (Sun et al. 2013). The pups were briefly anesthetized with a mixture of ketamine and xylazine. When unresponsive to stimulation, a cranial window was prepared and the exposed cortex loaded with the Ca^{2+} indicator rhod-2 AM. The analysis showed that compared to cortical astrocytes in anesthetized pups from the same litter, a significantly higher percentage of astrocytes in cortical slices 90 min after cutting responded to ATP (500 µM) (Fig. 4A) (232.4±19.7%, p<0.001, t test). This observation was not expected based on reduced immunolabeling of P2YR2 and P2YR4 observed in slices immersion-fixed 90 min after preparation (Fig. 3A–F). The potentiated response to ATP could reflect that slice preparation affected other steps in the purinergic signaling pathway, such as the interstitial volume (see below), the activity of ectonucleotidases involved in extracellular degradation

of ATP, IP$_3$ receptor activation, baseline cytosolic Ca^{2+} concentration, and the availability of the ER stores of Ca^{2+}, among others. In comparison, the number of astrocytes responding to the mGluR5 agonists, (±)-1-aminocyclopentane-trans-1,3-dicarboxylic acid (t-ACPD, 500 μM) and 3,5-dihydroxyphenylglycine (DHPG, 200 μM), were not significantly different *in vivo* vs. *ex vivo*, despite the marked upregulation of the intensity of immunolabeling of the mGluR5 receptors (p>0.5, t tests) (Fig. 4B–C). However, the amplitudes of Ca^{2+} signaling evoked by t-ACPD and DHPG were significantly reduced in acute slices compared to *in vivo* (p<0.001, t test). Combined, this analysis suggests that astrocytic receptor expression is sharply affected by preparation of acute slices. Moreover, Ca^{2+} mobilization in response to agonists was also distinctively different *in vivo* vs. *ex vivo*, and cannot be predicted by immunohistochemical analysis of receptor labeling because protein amounts need not reflect functional activity. A limitation of immunostaining intensity is that changes in epitope accessibility can alter staining intensity without changes in protein amount.

Loss of fine astrocytic processes in acute slices

Astrocytes retract a large fraction of their fine protrusions during the process of reactive gliosis (Oberheim et al. 2008; Sofroniew 2009). To determine the impact of slice preparations on the fine ultrastructure of astrocytes, the relative area occupied by astrocytic processes was quantified in hippocampal slices and compared to perfusion-fixed littermates using electron microscopy (EM) (Oberheim et al. 2009). We took advantage of the cytosolic protein GFP, which is present in even the finest astrocytic processes in hippocampus. Acute hippocampal slices were prepared from pups (P14–17) or adult (P56–66 old) GFAP-GFP mice (Zhuo et al. 1997) and fixed immediately (0 h), or following incubation in an oxygenated aCSF solution for 1 h or 3 h. Of note, only cells located a distance of 80–120 μm from the surface of the slice were analyzed. In perfusion-fixed tissue, GFP-positive astrocytic processes were elongated and irregularly shaped compared to previous descriptions (Lovatt et al. 2007; Oberheim et al. 2009; Peters et al. 1991) and often encased large mitochondria (Fig. 5A). Astrocytic processes occupied on average 20.5±0.9%, in young and 20.9±0.8%, in adult animals of the total area analyzed in perfusion-fixed sections (Fig. 5B). Strikingly, GFP-positive astrocytic processes only occupied 8.3±0.5% in young and 9.0±0.3% in adult slices immersion-fixed 1 h after isolation, and 7.2±0.4% in young and 9.1±0.4% in adult slices at 3 h after preparation. This represents 2.3–2.8-fold reductions in the relative area of GFP-positive processes (p<0.01, Kruskal-Wallis test with Dunn's test) (Fig. 5B). The GFP-positive processes in acute slices were short and rounded compared to perfusion-fixed tissue. Slices fixed immediately after preparation did not exhibit a significant reduction in the relative area of GFP-positive processes (p>0.05, Kruskal-Wallis test with Dunn's test) (Fig. 5A). This observation suggests that astrocytic processes shrink or retract during the first hours of incubation in oxygenated aCSF. It is also possible that immersion-fixation, which is a slow diffusional process compared to perfusion fixation, contributed to the apparent loss of astrocytic processes. In either case, a loss of astrocytic processes was evident in both the slices fixed at 1 and 3 h after preparation compared to the slices fixed immediately after vibratome cutting (0 h). Slices prepared from pups and adult mice, exhibited a similar degree of loss of astrocytic GFP-positive processes at all time points analyzed.

To use an alternative approach to evaluate whether astrocytes retract their fine processes in acute slices, the fine structure of the astrocytic plasma membrane was next analyzed using diolistic labeling (Oberheim et al. 2009; Oberheim et al. 2008) (Fig. 5C). We compared astrocytes in perfusion-fixed slices, as well as acutely-prepared slices immersion-fixed at 0, 1, and 3 h after preparation at a depth of 100–120 μm below the surface of the slices. The analysis of diolistic-labeled astrocytes supported the notion that astrocytic processes retracted during the first 1–3 h after preparation of the slices (Fig. 5D). Moreover, astrocytes located at the surface of the immersion-fixed section displayed a striking loss of their fine processes following 1 or 3 h incubation in oxygenated aCSF (Fig. 5D).

The volume of the interstitial space in acute slices

We next asked whether the interstitial space expanded in tandem with retraction of astrocytic processes. Quantification of cell-free areas in acute hippocampal slices revealed a significant increase in the size of interstitial space in both slices prepared from pups (P14–17) or adult (P56–66) mice (p<0.01, Kruskal-Wallis test with Dunn's test) (Fig. 6A–B). The increase in interstitial space occurred throughout all layers of the slice and was not an artifact of immersion fixation, because the relative area of empty space in slices fixed immediately after cutting (0 h) did not differ significantly from relative area of empty space in perfusion-fixed tissue (0.51±0.05% p>0.05 young, 0.21±0.01% p>0.05 adult; Kruskal-Wallis test with Dunn's test) (Fig. 6B).

However, it is recognized that the size of the interstitial space in fixed tissue may not reflect the interstitial space of live, intact tissue. Movement of fluid from the interstitial to the intracellular compartment (cell swelling) during the fixation process leaves little or no interstitial space in perfusion-fixed tissue and in tissue immersion-fixed immediately after vibratome sectioning (Peters et al. 1991). So why did slices fixed after 1 or 3 h incubation in an oxygenated aCSF exhibit a significant increase in the interstitial volume? We propose that extracellular proteases, activated by anoxia and traumatic injury during slice preparation, reduced cell-cell contacts and altered the extracellular matrix. A reduction of adhesion of the individual processes may result in reduced stretching during the fixation process and thereby an apparent increase in the extracellular space. Putative protease activity could also influence changes in antibody staining noted above.

To critically test whether the extracellular space displayed time-dependent volume changes *in vitro*, prior to fixation, we next employed the real-time iontophoretic tetramethylammonium (TMA) method comparing the interstitial volume fraction in acute slices after 1 h incubation in oxygenated aCSF with *in vivo* measurements obtained in anesthetized littermates (Nicholson 1992; Sykova and Nicholson 2008). The TMA method is based on measurement of the membrane-impermeant cation TMA^+ with a TMA^+ sensitive microelectrode located ~150 μm from another microelectrode, that then delivers TMA^+ by iontophoresis (Fig. 6C). Based on the slope and amplitude of the TMA^+ recordings, the interstitial volume fraction and tortuosity was calculated. We found, in accordance with earlier reports, that the volume fraction of the interstitial space (alpha) was comparable *ex vivo* and *in vivo* (Nicholson 1992; Sykova and Nicholson 2008) (p=0.27, t test) (Fig. 6D).

However, the tortuosity (lambda) was significantly decreased in acute slices compared with *in vivo* (p<0.001, t test) (Fig. 6D).

Thus, the recordings of the volume of the interstitial space in acute slices did not confirm the EM observation indicating that the interstital space was increased in slices immersion-fixed at 1 and 3 h relative to slices immersion-fixed at 0 hr. The reduced tortuosity of the extracellular space in the acute slice preparation is, however, consistent with the reduction of fine astrocytic processes noted in the immunoEM and diolistic labeling of astrocytes (Fig. 5D). A pausible explanation for the disparate findings using the two different techniques is that the interstitial space is lost in routine EM. Cellular swelling eliminates the interstitial space in tissue perfuson-fixed or immersion-fixed immediately after vibratome cutting. Activation of extracellular proteases in vibratome section incubated prior to immersion-fixation may degrade the extracellular matrix and cellular adhesion complexes, resulting in reduced cellular swelling in slices fixed after 1–3 hours incubation in oxygenated aCSF.

Slice preparation is linked to alteration in mitochondrial number and area

The immunoEM analysis also revealed that immersion-fixed slices exhibited a sharp drop in the number of mitochondria (p<0.01, Kruskal-Wallis test with Dunn's test) (Fig. 7A–B), concurrent with an increase in the average size of mitochondria in slices prepared from pups (P14–17) or adult (P56–66) GFAP-GFP mice (p<0.01, Kruskal-Wallis test with Dunn's test) (Fig. 7C). These changes in mitochondrial number and size were evident within both GFP$^+$ astrocytic processes and in GFP$^-$ processes from other cell types, including neurons, microglial cells, NG2 cells, and oligodendrocytes. Quantification of the average cross-sectional area of mitochondria in GFAP-GFP$^+$ processes showed that their decrease in numbers and increase in size was evident immediately after the slice preparation (Fig. 7B–C). Similar trends were noted in mitochondria located within other cell types, although the changes were slightly more modest (Fig. 7B–C). A calculation of percent area, occupied by all the mitochondria within GFP$^+$ astrocytic processes in the total area of the field, showed that the total area of mitochondria, within the processes of astrocytes and other cell types, remained relatively stable (Fig. 7D). This calculation suggests that mitochondria within the processes of all cells are mobile in the acutely-perfused slices, and that they fuse during the procedures associated with harvesting the brain and preparing the vibratome sections. One possibility is that long-lasting increases in cytosolic [Ca^{2+}] during slice preparation contributed to mitochondrial fusion (Duchen and Szabadkai 2010; Hom et al. 2007).

NADH imaging reveals distinct metabolic responses to K$^+$ in slices versus *in vivo*

The reduced co-enzyme nicotinamide adenine dinucleotide (NADH) has endogenous fluorescent properties that can be detected using 2-photon microscopy, while the oxidized co-enzyme (NAD$^+$) is not fluorescent. Intrinsic NADH fluorescence signals therefore provide a measure of the cellular redox-state. Earlier studies have shown rapid changes of NADH fluorescence in response to electrical stimulation in slices, and to spreading depression waves or sensory stimulation in anesthetized animals (Kasischke et al. 2011; Kasischke et al. 2004; Takano et al. 2007). An analysis of NADH fluorescence in vibratome slices prepared from GLT-1-GFP reporter mice revealed a higher NADH signal in GFP-positive astrocytes compared with other cells (Fig. 8A). This observation suggests that

NADH levels in slice preparations at baseline conditions are the highest in astrocytes, which is in accordance with an earlier report (Kasischke et al. 2004). The higher NADH fluorescence in astrocytes than in surrounding neuropil may reflect a more reduced basal state in fused mitochondria, since the mitochondrial dye rhodamine 123 co-localized with spots of high NADH fluorescence (Fig. 8B).

O_2 is delivered by the cerebral vasculature in live animals, whereas tissue slices receive O_2 from oxygenated aCSF during superfusion on the microscope stage. We next asked whether the different sources of O_2 affect the tissue redox state in response to a metabolic challenge. We compared changes in NADH signal in response to high K^+ *in vivo* and in slices. Extracellular K^+ was transiently increased by topical application of K^+ during continuous imaging of NADH. *In vivo*, elevation of K^+ induced a heterogeneous pattern of changes in NADH, similar to previous analysis of changes in NADH in response to spreading depression or whisker stimulation (Fig. 8C,D) (Kasischke et al. 2011; Takano et al. 2007). Perivascular tissue surrounding the cerebral vessels exhibited in a donut shape pattern a decrease in NADH signal (Fig. 8C,D). Concurrently, tissue located distant to the vasculature displays either no change, or a minor increase in NADH fluorescence. In contrast, the NADH signal in vibratome slices exhibited a uniform decrease in NADH signal in response to high K^+, which included both perivascular regions and those more distant to the vasculature (Fig. 8E,F). This observation is consistent with a scenario in which all parts of the tissue have equal access to O_2 and that K^+ therefore triggers a uniform decrease in NADH signal, suggesting that the fused mitochondria can respond to metabolic demand. In intact brain, the perivascular tissue has a privileged access to O_2 giving rise to a heterogeneous pattern of change in NADH signal. Perivascular tissue increases O_2 consumption and exhibits therefore a reduced NADH signal, whereas more distant regions (micro-watersheds) experience a relative O_2 deprivation and display an increase in NADH signal. Thus, this analysis indicates that the metabolic consequences of elevating K^+ in slices differ distinctively from those in the intact brain (Fig. 8C–F).

Acute hippocampal slices exhibit a sustained decrease in glycogen content

To obtain quantitative data for glycogen content in hippocampal slices, acute vibratome sections were also harvested for quantification of their glycogen and lactate contents (Cruz and Dienel 2002; Hertz et al. 2007). The analysis showed a sharp decrease in glycogen content in slices incubated in oxygenated aCSF at 21–24°C for 1 or 3 h, compared to slices harvested immediately after preparation (0 h) (p<0.01, Tukey-Kramer test) (Fig. 9A). Lactate concentration, on the other hand, decreased in slices incubated for 1 or 3 h in oxygenated aCSF, possibly reflecting diffusion and washout of slice-produced lactate into the aCSF (p<0.01, Tukey-Kramer test) (Fig. 9B). Thus, glycogen remained depleted during the entire observation period. In several studies, glycogen has been linked to synaptic plasticity *in vivo* (Gibbs et al. 2006; Suzuki et al. 2011). The permanent reduction in glycogen in acute slices may thereby have important implications for long-term potentiation (LTP), which is frequently employed for the study of synaptic plasticity in hippocampal slices.

Discussion

The main observation of this study is that astrocytes exhibit reactive changes shortly after preparation of acute hippocampal slices. Essentially all astrocytes in hippocampal slices re-express the developmental marker, nestin just 90 min after routine preparation of hippocampal slices with stable electrophysiological properties (Figs. 1–2). The immunoreactivities of Cx43 and AQP4 were markedly increased, concurrently with a relocation of their cellular distribution. Instead of a uniform dispersal of Cx43-positive plaques noted in perfusion-fixed brain tissue, intense Cx43 immunolabeling outlined the cell body and major processes of astrocytes in acute slices. The loss of the polarized expression of AQP4 in vascular astrocytic endfeet in slices was also striking. AQP4 redistributed to the cell bodies and major processes of astrocytes in acute slices, similar to Cx43. Neuronal markers, including MAP2, exhibited reduced immunolabeling near the surface of the slices, possibly reflecting neuronal injury (Fig. 3). Indeed, signal intensities of P2YR2, P2YR4, and mGluR5 were altered in slices, and Ca^{2+} responses to P2RY and mGluR5 receptor agonists (ATP, t-ACPD, and DHPG) differed from those observed *in vivo* (Fig. 4). Ultrastructural studies showed that astrocytes partly lost their fine protrusions resulting in an almost 3-fold reduction of the total area of GFAP-GFP-positive processes in acute slices. Confocal analysis of diolistic labeled astrocytes showed that astrocytes in vibratome sections, especially those close to the surface, rapidly lost their fine protrusions (Fig. 5). In parallel, the interstitial space expanded from less than 1% in perfusion-fixed tissue to 8–14% in vibratome slices immersion fixed 1 and 3 h after preparation (Fig. 6). The large volume of the interstitial space noted in hippocampal slices was not an artifact of immersion-fixation, since slices fixed immediately after cutting did not display a significant increase in the interstitial space. However, quantification of the extracellular space volume and tortuosity based on the TMA technique revealed that the extracellular space in the two preparations were comparable prior to fixation. The only detectable difference was a minor but significant decrease in tortuosity in acute slices compared to *in vivo* (Fig. 6). We have no direct explanation for these observations, but propose that extracellular proteases activated during preparations of the vibratome sections may reduce cellular adhesion, resulting in reduced stretching of astrocytic processes during the fixation process and thereby in an apparent reduction in their size in slices fixed at 1 and 3 h, but not at 0 h after vibratome cutting (Fig. 6). Another interesting observation was that the number of mitochondria decreased in parallel with an increase in the average cross-sectional area of mitochondria, suggesting that fusion of mitochondria may occur during vibratome slice preparation (Fig. 7). These changes of mitochondrial numbers and size were evident in both astrocytic (GFP$^+$) and non-astrocytic (GFP$^-$) processes. Moreover, imaging of NADH in live slices revealed large aggregates of mitochondria with high NADH fluorescence signals (Fig. 8). Changes in NADH fluorescence in response to high K$^+$ also differed markedly in the two preparations likely reflecting that intact brain tissue depends on O$_2$ delivery from the vasculature, whereas the aCSF superfusing of vibratome sections serves as the source of O$_2$ in slices (Fig. 8). Exposure to elevated K$^+$ uniformly decreased NADH signal in slices, possible reflecting an increase in the relative oxidative state. Since aCSF bathing the slice has much higher O$_2$ levels than tissue, the hypoxic response to K$^+$ in intact brain (detected as increased NADH signal in watershed regions) was blunted in the slices. Glycogen content

was reduced to ~ 1/3 after 1 h incubation of vibratome slices in oxygenated aCSF and showed no sign of recovery at 3 h even though the perfusate contained 10 mM glucose and energy metabolism was sufficiently robust to maintain stable fEPSCs during the same period (Fig. 9). These findings appear to contrast with normalization of glycogen granule number at 3h in the study in 21-day-old rats of Fiala et al. 2003, but numbers of glycogen particles cannot be equated with glycogen concentration because particles within the size range of 20–40 nm were counted by Fiala et al, and the volumes of particles in this range of size can differ by 8-fold due to volume dependence on the radius[3] of the particle. In the study by Lipton 1989, the initial depletion of glycogen concentration was followed by progressive increases with time, with normalization at 4h. cAMP can stimulate glycogenolysis, and its levels in slices from adult guinea pig hippocampus rise abruptly at the onset of incubation, but its concentration falls to low, stable levels between 2–8h in vitro (Whittingham et al. 1984), and cAMP is unlikely to explain differences in the extent of glycogen recovery in the present and Lipton studies. Conceivably, species differences (guinea pig vs. mouse vs. rat), age (not stated for guinea pigs vs. 14–17 day-old mouse pups vs. 21 day-old rats), slice preparative procedures (tissue chopper vs. vibratome), and slice incubation temperature could influence glycogen recovery time in the three studies. In the present study incubations were carried out at 21–24°C, whereas higher temperatures used in the other studies (32°C, Fiala et al., 2003 and 36°C, Lipton, 1989) may have accelerated metabolic recovery. There are substantial developmental changes in metabolic capacity prior to and shortly after weaning that can have a high impact on substrate utilization by brain slices derived from animals of different ages (Dienel 2012), and guinea pigs are known to have advanced brain development compared with rats and mice (Booth et al. 1980). Enzymes of glycogen metabolism increase markedly during the postnatal period (Knull and Khandelwal 1982; Pfeiffer et al. 1993), and lower levels of glucose utilization enzymes may increase slice dependence on glycogen as an energy source, and lower glycogen biosynthetic capacity in slices from younger animals may underlie slower recovery compared with slices from older animals.

Combined, these observations are of wide interest for studies based on acute slices, such as electrophysiological investigations of synaptic transmission and neuroglia signaling. While slices often are used in the analysis of synaptic functions and neural circuits, it should be acknowledged that cellular metabolism and receptor expression does not reflect *in vivo* conditions, particularly in slices from immature animals that will undergo substantial developmental changes until reaching the adult state. Most importantly, astrocytes, which are critical for support of synapses, display reactive changes as early as 60 min after preparation of the slices. Significant changes in the expression and subcellular location of several key astrocytic proteins (i.e. GFAP, Cx43 and AQP4) were documented. In addition, agonist-induced astrocytic Ca^{2+} signaling differed in slices compared to *in vivo*. Several other observations suggest that communication between neurons and astrocytes in slices may differ from that *in vivo*. For example, the loss of fine astrocytic protrusions is likely linked to reduced glia coverage of synapses, which may contribute to abnormal K^+ homeostasis and glutamate spillover due to less efficient glutamate uptake. It is also possible that changes in the extracellular matrix and cell adhesion interfere with cell-cell signaling and perhaps create signaling pathways that are not operative *in vivo*. A striking example of

how different slices vs. intact brain responded to stimulation was the change in the NADH fluorescence elicited by elevation of extracellular K^+. While slices display a uniform decrease in NADH signal, likely reflecting increased oxidative metabolism, the responses *in vivo* were complex with perivascular region also exhibiting a decrease, while the NADH signal increased in microwatershed regions.

Over the past decade, studies combining imaging of Ca^{2+} signaling with patch recordings have led to the discovery that bi-directional communication occurs between astrocytes and neurons (Nedergaard and Verkhratsky 2012). These studies have documented that astrocytes, via Ca^{2+}-dependent gliotransmitter release, are actively involved in complex synaptic functions that previously had been regarded as strictly neuronal. More recent work has questioned whether gliotransmitter release occurs during physiological conditions and suggested that astrocytic release of glutamate is restricted to pathological conditions or suprathreshold stimulation. For discussion of these topics, please refer to recent reviews (Agulhon et al. 2008; Nedergaard and Verkhratsky 2012). Since data in favor and against the existence of gliotransmission have been collected mostly in acute slices from immature rodents, it is important to note that astrocytes, as the principle supportive cell in CNS, exhibit a striking sensitivity to changes in their environment. In fact simply touching a single astrocyte with a patch pipette without breaking the plasma membrane is sufficient to evoke release of vasoactive compounds and dilatation of nearby vessels (Zonta et al. 2003). Thus, it is possible that even minor differences in how hippocampal slices are prepared will alter neuroglia signaling pathways and thereby contribute to the documented observation variability from one lab to another.

Microglial cells, another non-neuronal cell type in CNS, are also activated in acute slices. It is in this regard that *in vivo* studies have shown that chemotaxis of microglial cell processes in response to local injury is mediated by ATP released from astrocytes (Haynes et al. 2006; Koizumi et al. 2013). ATP is released in response to traumatic injury (Abbracchio et al. 2009; Wang et al. 2004) and the tissue injury inflicted by the vibratome likely directly activates microglial cells. In addition, the upregulation of Cx43 noted in the slices (Fig. 2G–I) may contribute to continued activation of microglial cells. Earlier studies have shown that inhibitors of hemichannels suppress both astrocytic ATP release and microglial cell motility (Haynes et al. 2006). Purinergic activation of microglia is known to induce maturation and release of several cytokines and chemokines, including IL-1 (for reviews see (Kettenmann et al. 2011; Ransohoff and Engelhardt 2012)). Many of these cytokines are known to modulate synaptic transmission (Galic et al. 2012), as well as trigger reactive changes in astrocytes (Sofroniew 2009; Verkhratsky et al. 2012). Multiple mechanisms involving glial cells may therefore contribute to rapid changes in synaptic transmission in acute hippocampal slices (Torres et al. 2012). It is in this regard important to note that astrogliosis may differ from laboratorium to laboratorium depending on the exact procedures, solutions, and other conditions under which the slices are prepared. However, the fact that marked reactive astro- and microgliosis are evident 90 min after slice preparation following standard procedure in slices that by electrophysiological measures are healthy suggests that glial cells may tolerate the procedure less well than neurons. Additional studies are clearly needed to address the functional significance of astro- and microgliosis on synaptic plasticity in acute hippocampal

slices. Based on this analysis and the fact that many manipulations can only be done *ex vivo*, we suggest that data obtained in slice preparation at least in part are confirmed *in vivo*. Nevertheless, since preparation of cranial windows also alters the physiological state of astrocytes and microglial cells, it is important to critically evaluate and minimize the extent of gliosis in any preparation used in the study of neuro-glia signaling.

Acknowledgments

References

Abbracchio MP, Burnstock G, Verkhratsky A, Zimmermann H. Purinergic signalling in the nervous system: an overview. Trends Neurosci. 2009; 32:19–29. [PubMed: 19008000]

Agulhon C, Petravicz J, McMullen AB, Sweger EJ, Minton SK, Taves SR, Casper KB, Fiacco TA, McCarthy KD. What is the role of astrocyte calcium in neurophysiology? Neuron. 2008; 59:932–946. [PubMed: 18817732]

Aitken PG, Breese GR, Dudek FF, Edwards F, Espanol MT, Larkman PM, Lipton P, Newman GC, Nowak TS Jr, Panizzon KL, et al. Preparative methods for brain slices: a discussion. J Neurosci Methods. 1995; 59:139–149. [PubMed: 7475244]

Allen NJ, Barres BA. Neuroscience: Glia - more than just brain glue. Nature. 2009; 457:675–677. [PubMed: 19194443]

Ball KK, Gandhi GK, Thrash J, Cruz NF, Dienel GA. Astrocytic connexin distributions and rapid, extensive dye transfer via gap junctions in the inferior colliculus: implications for [(14)C]glucose metabolite trafficking. J Neurosci Res. 2007; 85:3267–3283. [PubMed: 17600824]

Bekar L, Libionka W, Tian GF, Xu Q, Torres A, Wang X, Lovatt D, Williams E, Takano T, Schnermann J, et al. Adenosine is crucial for deep brain stimulation-mediated attenuation of tremor. Nat Med. 2008; 14:75–80. [PubMed: 18157140]

Booth RF, Patel TB, Clark JB. The development of enzymes of energy metabolism in the brain of a precocial (guinea pig) and non-precocial (rat) species. J Neurochem. 1980; 34:17–25. [PubMed: 6108983]

Brown TH, Chapman PF, Kairiss EW, Keenan CL. Long-term synaptic potentiation. Science. 1988; 242:724–728. [PubMed: 2903551]

Clarke SR, Shetty AK, Bradley JL, Turner DA. Reactive astrocytes express the embryonic intermediate neurofilament nestin. Neuroreport. 1994; 5:1885–1888. [PubMed: 7841369]

Cotrina ML, Lin JH, Alves-Rodrigues A, Liu S, Li J, Azmi-Ghadimi H, Kang J, Naus CC, Nedergaard M. Connexins regulate calcium signaling by controlling ATP release. Proc Natl Acad Sci U S A. 1998; 95:15735–15740. [PubMed: 9861039]

Cruz NF, Dienel GA. High glycogen levels in brains of rats with minimal environmental stimuli: implications for metabolic contributions of working astrocytes. J Cereb Blood Flow Metab. 2002; 22:1476–1489. [PubMed: 12468892]

Dermietzel R, Traub O, Hwang TK, Beyer E, Bennett MV, Spray DC, Willecke K. Differential expression of three gap junction proteins in developing and mature brain tissues. Proc Natl Acad Sci U S A. 1989; 86:10148–10152. [PubMed: 2557621]

Dienel GA. Fueling and imaging brain activation. ASN NEURO. 2012; 4:e00093. [PubMed: 22612861]

Dienel GA, Wang RY, Cruz NF. Generalized sensory stimulation of conscious rats increases labeling of oxidative pathways of glucose metabolism when the brain glucose-oxygen uptake ratio rises. J Cereb Blood Flow Metab. 2002; 22:1490–1502. [PubMed: 12468893]

Dodt HU, Zieglgansberger W. Visualizing unstained neurons in living brain slices by infrared DIC-videomicroscopy. Brain Res. 1990; 537:333–336. [PubMed: 2085783]

Duchen MR, Szabadkai G. Roles of mitochondria in human disease. Essays Biochem. 2010; 47:115–137. [PubMed: 20533904]

Edwards FA, Konnerth A, Sakmann B, Takahashi T. A thin slice preparation for patch clamp recordings from neurones of the mammalian central nervous system. Pflugers Arch. 1989; 414:600–612. [PubMed: 2780225]

Fiala JC, Kirov SA, Feinberg MD, Petrak LJ, George P, Goddard CA, Harris KM. Timing of neuronal and glial ultrastructure disruption during brain slice preparation and recovery in vitro. The Journal of comparative neurology. 2003; 465:90–103. [PubMed: 12926018]

Franke H, Verkhratsky A, Burnstock G, Illes P. Pathophysiology of astroglial purinergic signalling. Purinergic Signal. 2012; 8:629–657. [PubMed: 22544529]

Galic MA, Riazi K, Pittman QJ. Cytokines and brain excitability. Front Neuroendocrinol. 2012; 33:116–125. [PubMed: 22214786]

Gibbs ME, Anderson DG, Hertz L. Inhibition of glycogenolysis in astrocytes interrupts memory consolidation in young chickens. Glia. 2006; 54:214–222. [PubMed: 16819764]

Guthrie PB, Knappenberger J, Segal M, Bennett MV, Charles AC, Kater SB. ATP released from astrocytes mediates glial calcium waves. J Neurosci. 1999; 19:520–528. [PubMed: 9880572]

Haynes SE, Hollopeter G, Yang G, Kurpius D, Dailey ME, Gan WB, Julius D. The P2Y12 receptor regulates microglial activation by extracellular nucleotides. Nat Neurosci. 2006; 9:1512–1519. [PubMed: 17115040]

Hertz L, Peng L, Dienel GA. Energy metabolism in astrocytes: high rate of oxidative metabolism and spatiotemporal dependence on glycolysis/glycogenolysis. J Cereb Blood Flow Metab. 2007; 27:219–249. [PubMed: 16835632]

Hom JR, Gewandter JS, Michael L, Sheu SS, Yoon Y. Thapsigargin induces biphasic fragmentation of mitochondria through calcium-mediated mitochondrial fission and apoptosis. J Cell Physiol. 2007; 212:498–508. [PubMed: 17443673]

Huang C, Han X, Li X, Lam E, Peng W, Lou N, Torres A, Yang M, Garre JM, Tian GF, et al. Critical role of connexin 43 in secondary expansion of traumatic spinal cord injury. J Neurosci. 2012; 32:3333–3338. [PubMed: 22399755]

Iliff JJ, Wang M, Liao Y, Plogg BA, Peng W, Gundersen GA, Benveniste H, Vates GE, Deane R, Goldman SA, et al. A paravascular pathway facilitates CSF flow through the brain parenchyma and the clearance of interstitial solutes, including amyloid beta. Sci Transl Med. 2012; 4:147ra111.

Kaneko Y, Tajiri N, Yu S, Hayashi T, Stahl CE, Bae E, Mestre H, Franzese N, Rodrigues A Jr, Rodrigues MC, et al. Nestin overexpression precedes caspase-3 upregulation in rats exposed to controlled cortical impact traumatic brain injury. Cell Med. 2012; 4:55–63. [PubMed: 23101029]

Kang J, Jiang L, Goldman SA, Nedergaard M. Astrocyte-mediated potentiation of inhibitory synaptic transmission. Nat Neurosci. 1998; 1:683–692. [PubMed: 10196584]

Kasischke KA, Lambert EM, Panepento B, Sun A, Gelbard HA, Burgess RW, Foster TH, Nedergaard M. Two-photon NADH imaging exposes boundaries of oxygen diffusion in cortical vascular supply regions. J Cereb Blood Flow Metab. 2011; 31:68–81. [PubMed: 20859293]

Kasischke KA, Vishwasrao HD, Fisher PJ, Zipfel WR, Webb WW. Neural activity triggers neuronal oxidative metabolism followed by astrocytic glycolysis. Science. 2004; 305:99–103. [PubMed: 15232110]

Kettenmann H, Hanisch UK, Noda M, Verkhratsky A. Physiology of microglia. Physiol Rev. 2011; 91:461–553. [PubMed: 21527731]

Kimelberg HK. Supportive or information-processing functions of the mature protoplasmic astrocyte in the mammalian CNS? A critical appraisal. Neuron glia biology. 2007; 3:181–189. [PubMed: 18545675]

Knull HR, Khandelwal RL. Glycogen metabolizing enzymes in brain. Neurochem Res. 1982; 7:1307–1317. [PubMed: 6218421]

Koizumi S, Ohsawa K, Inoue K, Kohsaka S. Purinergic receptors in microglia: functional modal shifts of microglia mediated by P2 and P1 receptors. Glia. 2013; 61:47–54. [PubMed: 22674620]

Langmoen, I.; Anderson, P. The hippocampal slice in vitro. A description of the technique and some examples of the opportunities it offers. In: Kerkut, GAWH., editor. Electrophysiology of Isolated Mammalian CNS Preparations. New York: Academic Press; 1981. p. 51-105.

Li Y, Chopp M. Temporal profile of nestin expression after focal cerebral ischemia in adult rat. Brain Res. 1999; 838:1–10. [PubMed: 10446310]

Liem RK, Messing A. Dysfunctions of neuronal and glial intermediate filaments in disease. J Clin Invest. 2009; 119:1814–1824. [PubMed: 19587456]

Lin JH, Lou N, Kang N, Takano T, Hu F, Han X, Xu Q, Lovatt D, Torres A, Willecke K, et al. A central role of connexin 43 in hypoxic preconditioning. J Neurosci. 2008; 28:681–695. [PubMed: 18199768]

Lipton P. Regulation of glycogen in the dentate gyrus of the in vitro guinea pig hippocampus; effect of combined deprivation of glucose and oxygen. J Neurosci Methods. 1989; 28:147–154. [PubMed: 2471020]

Lipton P, Aitken PG, Dudek FE, Eskessen K, Espanol MT, Ferchmin PA, Kelly JB, Kreisman NR, Landfield PW, Larkman PM, et al. Making the best of brain slices: comparing preparative methods. J Neurosci Methods. 1995; 59:151–156. [PubMed: 7475245]

Llano I, Marty A, Johnson JW, Ascher P, Gahwiler BH. Patch-clamp recording of amino acid-activated responses in "organotypic" slice cultures. Proc Natl Acad Sci U S A. 1988; 85:3221–3225. [PubMed: 2834737]

Lovatt D, Sonnewald U, Waagepetersen HS, Schousboe A, He W, Lin JH, Han X, Takano T, Wang S, Sim FJ, et al. The transcriptome and metabolic gene signature of protoplasmic astrocytes in the adult murine cortex. J Neurosci. 2007; 27:12255–12266. [PubMed: 17989291]

Mathiisen TM, Lehre KP, Danbolt NC, Ottersen OP. The perivascular astroglial sheath provides a complete covering of the brain microvessels: an electron microscopic 3D reconstruction. Glia. 2010; 58:1094–1103. [PubMed: 20468051]

Nakase T, Yoshida Y, Nagata K. Enhanced connexin 43 immunoreactivity in penumbral areas in the human brain following ischemia. Glia. 2006; 54:369–375. [PubMed: 16886200]

Nedergaard M, Verkhratsky A. Artifact versus reality--how astrocytes contribute to synaptic events. Glia. 2012; 60:1013–1023. [PubMed: 22228580]

Neher E, Sakmann B. Single-channel currents recorded from membrane of denervated frog muscle fibres. Nature. 1976; 260:799–802. [PubMed: 1083489]

Nicholson C. Quantitative analysis of extracellular space using the method of TMA+ iontophoresis and the issue of TMA+ uptake. Canadian journal of physiology and pharmacology. 1992; 70(Suppl):S314–S322. [PubMed: 1295682]

Nicholson C, Kamali-Zare P, Tao L. Brain extracellular space as a diffusion barrier. Comput Visual Sci. 2011; 14:309–325. [PubMed: 23172993]

Nielsen S, Nagelhus EA, Amiry-Moghaddam M, Bourque C, Agre P, Ottersen OP. Specialized membrane domains for water transport in glial cells: high-resolution immunogold cytochemistry of aquaporin-4 in rat brain. J Neurosci. 1997; 17:171–180. [PubMed: 8987746]

Oberheim NA, Takano T, Han X, He W, Lin JH, Wang F, Xu Q, Wyatt JD, Pilcher W, Ojemann JG, et al. Uniquely hominid features of adult human astrocytes. J Neurosci. 2009; 29:3276–3287. [PubMed: 19279265]

Oberheim NA, Tian GF, Han X, Peng W, Takano T, Ransom B, Nedergaard M. Loss of astrocytic domain organization in the epileptic brain. J Neurosci. 2008; 28:3264–3276. [PubMed: 18367594]

Peters, A.; Palay, SL.; Webster, HD. The fine structure of the nervous system : neurons and their supporting cells. New York: Oxford University Press; 1991.

Pfeiffer B, Buse E, Meyermann R, Rocha MJ, Hamprecht B. Glycogen phosphorylase activity and immunoreactivity during pre- and postnatal development of rat brain. Histochemistry. 1993; 100:265–270. [PubMed: 8276640]

Ransohoff RM, Engelhardt B. The anatomical and cellular basis of immune surveillance in the central nervous system. Nat Rev Immunol. 2012; 12:623–635. [PubMed: 22903150]

Regan MR, Huang YH, Kim YS, Dykes-Hoberg MI, Jin L, Watkins AM, Bergles DE, Rothstein JD. Variations in promoter activity reveal a differential expression and physiology of glutamate transporters by glia in the developing and mature CNS. J Neurosci. 2007; 27:6607–6619. [PubMed: 17581948]

Richard, CD. The preparation of brain tissue slices for electrophysiological studies. In: Wheal, GAKaHV., editor. Electrophysiology of Isolated Mammalian CNS Preparations. New York: Academic Press; 1981. p. 107-132.

Sarvey JM, Burgard EC, Decker G. Long-term potentiation: studies in the hippocampal slice. J Neurosci Methods. 1989; 28:109–124. [PubMed: 2542698]

Schwartzkroin PA, Wester K. Long-lasting facilitation of a synaptic potential following tetanization in the in vitro hippocampal slice. Brain Res. 1975; 89:107–119. [PubMed: 167909]

Sigworth FJ, Neher E. Single Na+ channel currents observed in cultured rat muscle cells. Nature. 1980; 287:447–449. [PubMed: 6253802]

Skrede K, Westgaard R. The transverse hippocampal slice: a well-defined cortical structure maintained in vitro. Brain Res Bull. 1971; 5:391–403.

Sofroniew MV. Molecular dissection of reactive astrogliosis and glial scar formation. Trends Neurosci. 2009; 32:638–647. [PubMed: 19782411]

Sun W, McConnell E, Pare JF, Xu Q, Chen M, Peng W, Lovatt D, Han X, Smith Y, Nedergaard M. Glutamate-dependent neuroglial calcium signaling differs between young and adult brain. Science. 2013; 339:197–200. [PubMed: 23307741]

Suzuki A, Stern SA, Bozdagi O, Huntley GW, Walker RH, Magistretti PJ, Alberini CM. Astrocyte-neuron lactate transport is required for long-term memory formation. Cell. 2011; 144:810–823. [PubMed: 21376239]

Sykova E, Nicholson C. Diffusion in brain extracellular space. Physiological reviews. 2008; 88:1277–1340. [PubMed: 18923183]

Takano T, Tian GF, Peng W, Lou N, Lovatt D, Hansen AJ, Kasischke KA, Nedergaard M. Cortical spreading depression causes and coincides with tissue hypoxia. Nat Neurosci. 2007; 10:754–762. [PubMed: 17468748]

Torres A, Wang F, Xu Q, Fujita T, Dobrowolski R, Willecke K, Takano T, Nedergaard M. Extracellular Ca(2)(+) acts as a mediator of communication from neurons to glia. Science signaling. 2012; 5:ra8. [PubMed: 22275221]

Tulapurkar ME, Zundorf G, Reiser G. Internalization and desensitization of a green fluorescent protein-tagged P2Y nucleotide receptor are differently controlled by inhibition of calmodulin-dependent protein kinase II. J Neurochem. 2006; 96:624–634. [PubMed: 16405509]

VanSlyke JK, Musil LS. Cytosolic stress reduces degradation of connexin43 internalized from the cell surface and enhances gap junction formation and function. Molecular biology of the cell. 2005; 16:5247–5257. [PubMed: 16135529]

Verkhratsky A, Sofroniew MV, Messing A, deLanerolle NC, Rempe D, Rodriguez JJ, Nedergaard M. Neurological diseases as primary gliopathies: a reassessment of neurocentrism. ASN Neuro. 2012; 4

Wang X, Arcuino G, Takano T, Lin J, Peng WG, Wan P, Li P, Xu Q, Liu QS, Goldman SA, et al. P2X7 receptor inhibition improves recovery after spinal cord injury. Nat Med. 2004; 10:821–827. [PubMed: 15258577]

Whittingham TS, Lust WD, Christakis DA, Passonneau JV. Metabolic stability of hippocampal slice preparations during prolonged incubation. J Neurochem. 1984; 43:689–696. [PubMed: 6086837]

Yamamoto, c; McIlwain, H. Electrical activities in thin sections from the mammalian brain maintained in chemically defined media in vitro. J Neurochem. 1966; 13:1333–1343. [PubMed: 5962016]

Zhuo L, Sun B, Zhang CL, Fine A, Chiu SY, Messing A. Live astrocytes visualized by green fluorescent protein in transgenic mice. Dev Biol. 1997; 187:36–42. [PubMed: 9224672]

Zonta M, Angulo MC, Gobbo S, Rosengarten B, Hossmann KA, Pozzan T, Carmignoto G. Neuron-to-astrocyte signaling is central to the dynamic control of brain microcirculation. Nat Neurosci. 2003; 6:43–50. [PubMed: 12469126]
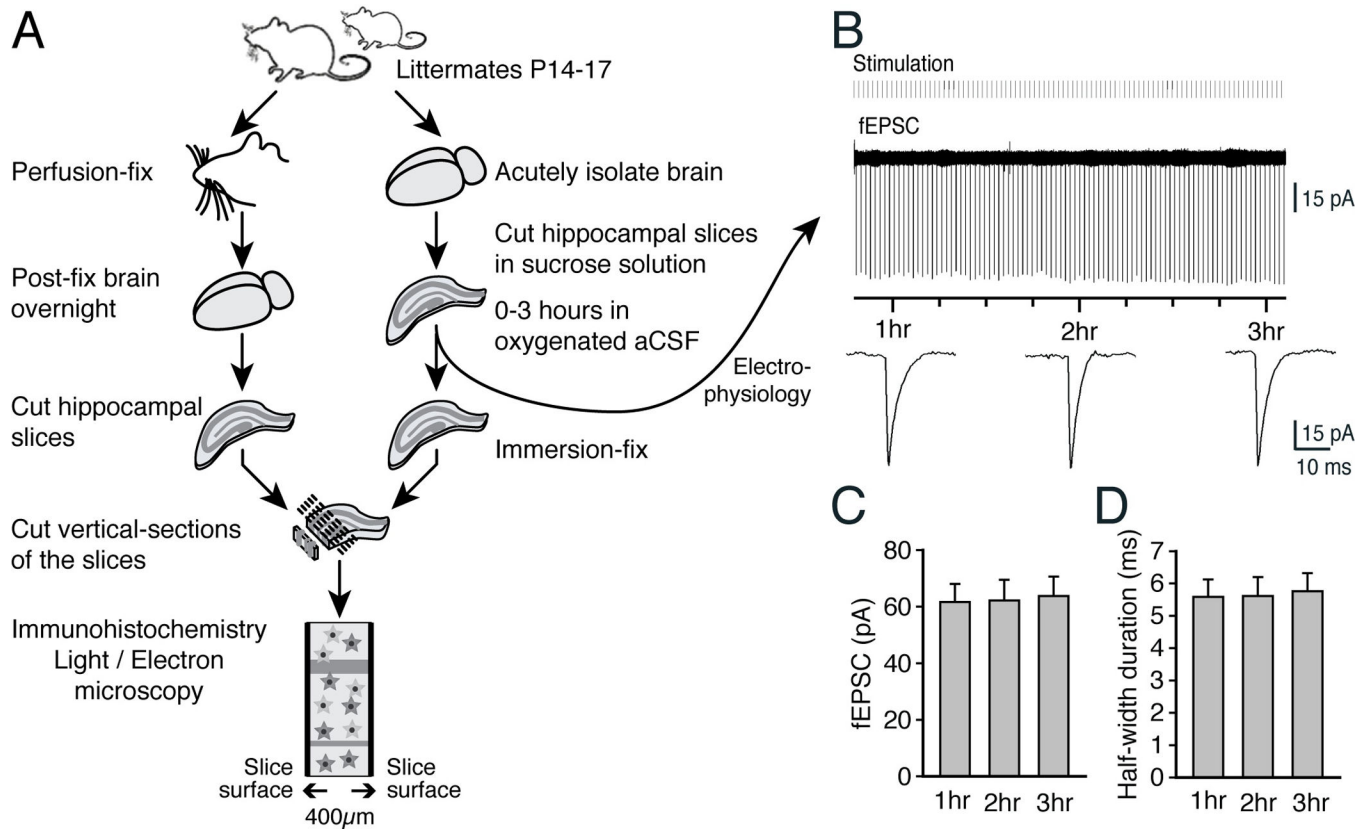
Fig. 1. Schematic outline of the experiments

(**A**) Littermates were used in parallel for the preparation of perfusion fixation or acute hippocampal slices that were immersion-fixed after 0 or 60–180 min incubation in oxygenated aCSF, followed by regular immunohistochemistry. Selected vibratome slices were synchronously used for recordings of evoked field excitatory postsynaptic current (fEPSC). (**B**) Representative traces of field fEPSC in an acute hippocampal slice. Recordings were initiated 1 h after vibratome preparation of the slices. The recordings showed that fEPSC remained stable for the 2 h of recordings. (**C,D**) Histograms comparing the amplitudes and half-width durations of fEPSC in all experiments (N=5, Mean ± sem, P>0.5, ANOVA).
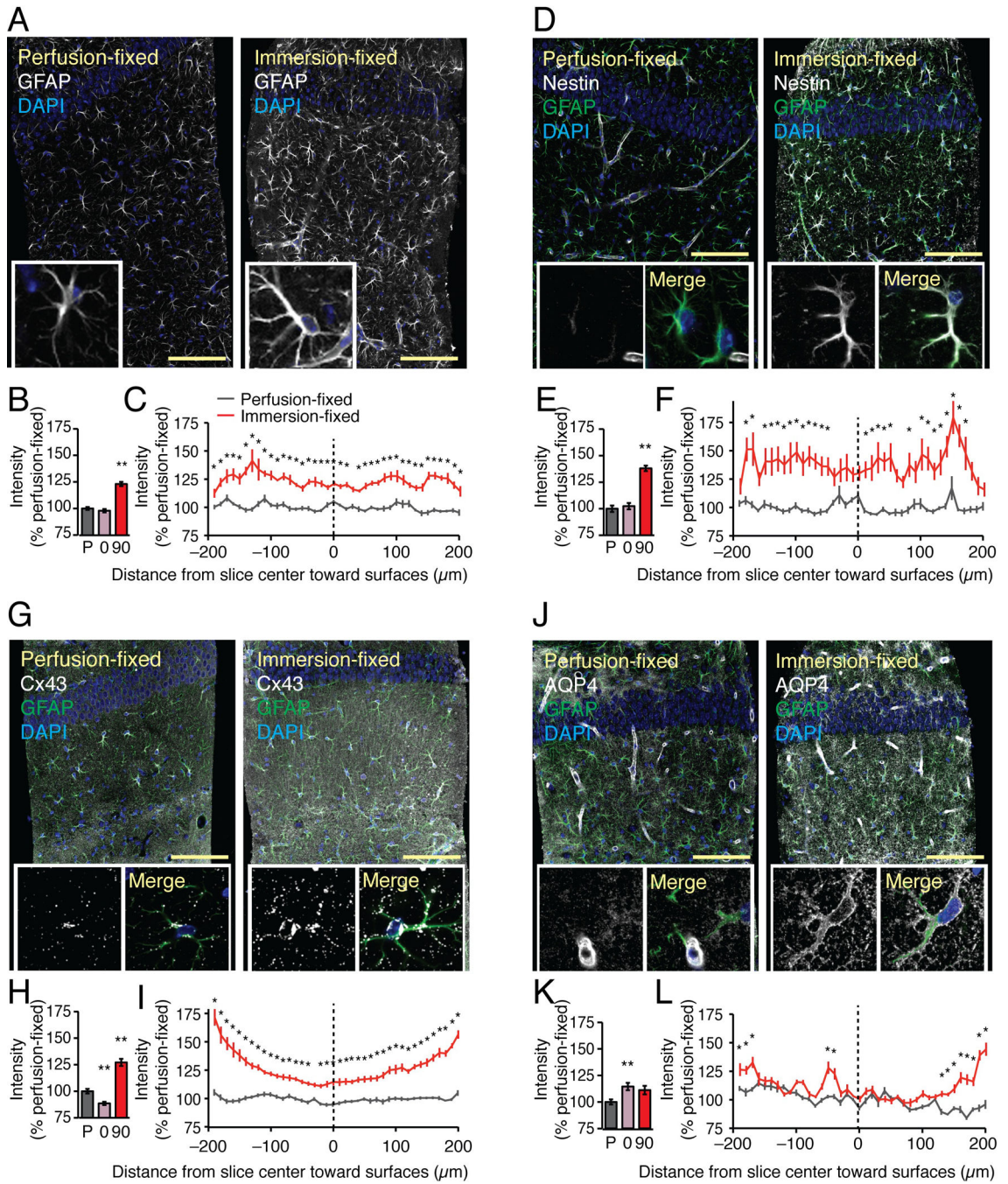
Fig. 2. Classical signs of reactive astrogliosis are evident in acute hippocampal slices
Comparisons of immunolabeling of GFAP, nestin, Cx43, and AQP4 in acute hippocampal slices immersion-fixed in 4% paraformaldehyde at 0 or 90 min after vibratome cutting with brains from littermates that were perfusion-fixed. All brains were harvested from 14–17 day old mouse pups. (**A**) GFAP immunolabeling exhibited a modest increase in slices immersion-fixed at 90 min compared with perfusion-fixed slices. Scale bar, 100 μm. Blue is DAPI stained nuclei. *Insert*: High magnification view of single astrocyte. (**B**) A histogram comparing GFAP immuno-fluorescence intensities of perfusion-fixed slices (P) with slices

that were immersion-fixed immediately after vibratome cutting (0), and 90 min after cutting (90) (N=20, Mean ± sem, **, P < 0.01, ANOVA with Tukey-Kramer test). (**C**) GFAP intensity profile from surface to surface across the 400 μm-thick perfusion-fixed slices (black) and immersion-fixed slices (red). The intensity values of each position were normalized to overall intensity of the perfusion-fixed slice (N=10, Mean ± sem, *, P < 0.05, ANOVA with Tukey-Kramer test). (**D-F**) Nestin was only expressed in endothelial cells in perfusion-fixed slices, whereas essentially all astrocytes in slices immersion-fixed 90 min after preparation were nestin-positive (N=20, Mean ± sem, **, P < 0.01, ANOVA with Tukey-Kramer test). The slices were co-labeled with GFAP (green) and DAPI (blue), also shown in Merge image of one astrocyte. (**G–I**) The predominant astrocytic gap junction protein, Cx43, was distributed in small evenly distributed plaques in perfusion-fixed brain. A striking increase in number and size of Cx43-positive plaques was evident in acute vibratome sections fixed at 90 min. Quantification of the overall Cx43 immunofluoresence showed a significant increase in slices fixed at 90 min, with a trend toward the highest expression just below the surface of the slices (N=20, Mean ± sem, **, P < 0.01, ANOVA with Tukey-Kramer test). The slices were co-labeled with GFAP (green) and DAPI (blue), also shown in Merge image. (**J–L**) The astrocytic water channel, AQP4, is typically localized in astrocytic vascular endfeet in intact tissue. In vibratome sections, AQP4 redistributed and outlined the cell body and major astrocytic processes giving rise to a less polarized vascular distribution (N=20, Mean ± sem, **, P < 0.01, ANOVA with Tukey-Kramer test). The slices were co-labeled with GFAP (green) and DAPI (blue), also shown in Merge image of a single astrocyte.
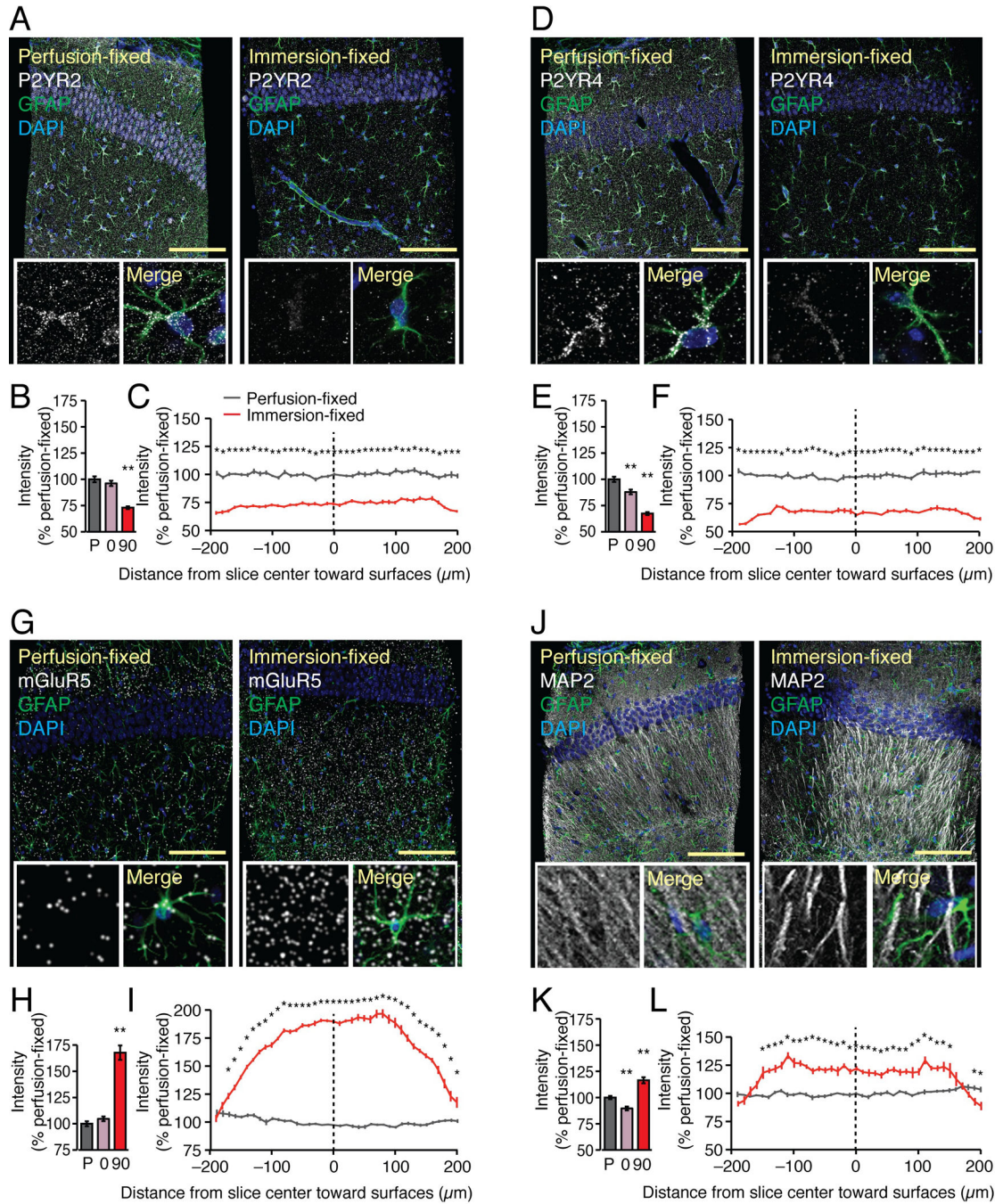
Fig. 3. Changes in immunolabeling of astrocytic receptors in acute hippocampal slices
Immunolabeling against P2YR2, P2YR4, mGluR5, and MAP2 were compared in acute
hippocampal slices immersion-fixed in 4% paraformaldehyde 0 or 90 min after vibratome
cutting with perfusion-fixed brains of 14–17 day-old mouse pups. (**A**) The purinergic
receptor P2YR2 was evenly distributed across perfusion-fixed section with a somewhat
higher density in cell bodies and vascular processes of astrocytes. A general decrease in
P2YR2 immunolabeling was noted in slices immersion-fixed 90 min after preparation. Scale
bar, 100 μm. Tissue was also co-stained with GFAP (green) and DAPI (blue). *Insert*: High

magnification view of single astrocyte. Merge image shows GFAP (green) and DAPI (blue) as well. (**B**) A histogram showing overall P2YR2 immuno-fluorescence intensities of perfusion-fixed tissue (P), tissue that was immersion-fixed immediately after vibratome cutting (O), and acutely isolated tissue fixed at 90 min after cutting (A). (N=20, Mean ± sem, **, P < 0.01, ANOVA with Tukey-Kramer test). (**C**) P2YR2 immuno-fluorescence intensity across from a surface to surface of the 400 μm thickness of the perfusion-fixed slice (black) and acute slice (red) normalized to the overall intensity of the perfusion-fixed slice (N=10, Mean ± sem, *, P < 0.05, ANOVA with Tukey-Kramer test). (**D–F**) Similarly, P2YR4 immunolabeling was significantly reduced in slices immersion-fixed at both 0 and 90 min (N=20, Mean ± sem, **, P < 0.01, ANOVA with Tukey-Kramer test). The slices were co-labeled with GFAP (green) and DAPI (blue), also shown in Merge image. (**G–I**) The Gq-coupled metabotropic glutamate receptor, mGluR5, exhibited a striking increase in immunolabeling in vibratome slices. The expression was highest in the center of the slices (N=20, Mean ± sem, **, P < 0.01, ANOVA with Tukey-Kramer test). The slices were co-labeled with GFAP (green) and DAPI (blue), also shown in Merge image. (**J–L**) The neuronal marker, MAP2 outlined CA1 pyramidal neurons dendrites in stratum radiatum in perfusion-fixed slices. A loss of MAP2 immunolabeling was evident in tissue close to the surfaces of the slices (N=20, Mean ± sem, **, P < 0.01, ANOVA with Tukey-Kramer test). The slices were co-labeled with GFAP (green) and DAPI (blue), also shown in Merge image.
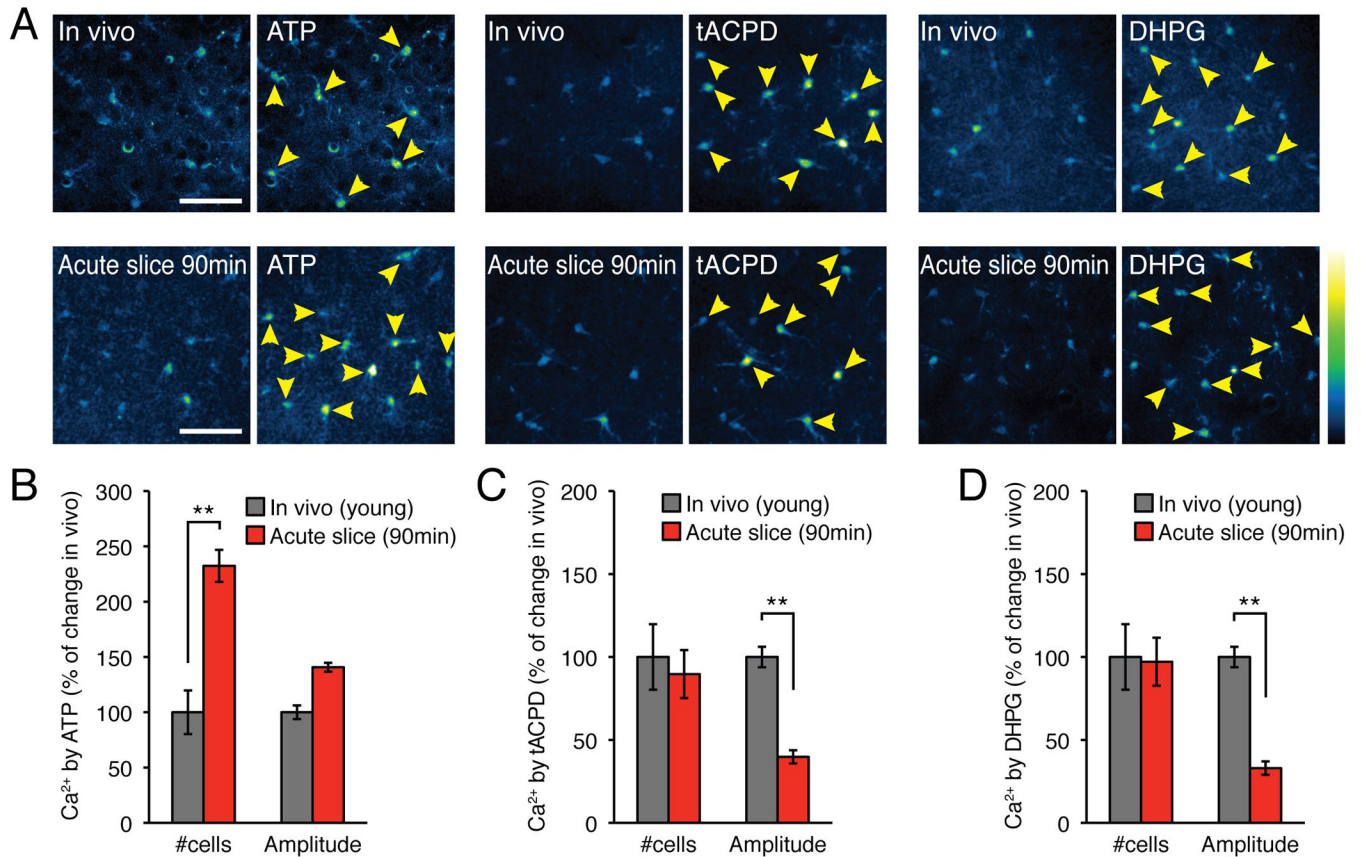
Fig. 4. Agonists trigger distinctly different Ca²⁺ responses in cortical astrocytes *in vivo* vs. *ex vivo*

Comparison of agonist induced Ca²⁺ increases in cortical astrocytes in acute slices (90 min after cutting) and *in vivo* of 14–17 day old mouse pups. Both preparations were loaded with the Ca²⁺ indicator rhod-2 AM (5 μM). Ca²⁺ responses in slices were normalized to *in vivo* data. (**A**) Representative examples of Ca²⁺ increases *in vivo* vs. in acute slices (90 min) evoked by the agonists, ATP (500 μM), tACPD (500 μM), and DHPG (200 μM). Yellow arrows indicate astrocytes that increased rhod-2 fluorescence signal by more than 20%. (**B**) Histogram comparing the number of astrocytes responding to the purine receptor agonist ATP (N=4–10 animals for *vivo* and N=8 slices from 3 animals, Mean ± sem, *, p < 0.05, **, p < 0.01, t tests). (**C**) Comparison of responses to the mGluR5 agonist t-ACPD (N=10–11 animals for *vivo* and N=9–10 slices from 3–4 animals, Mean ± sem, **, p < 0.01, t tests). (**D**) Comparison of responses to the mGluR5 agonist DHPG (N=8–13 animals for *vivo* and N=8 slices from 4 animals, Mean ± sem, **, p < 0.01, t test).
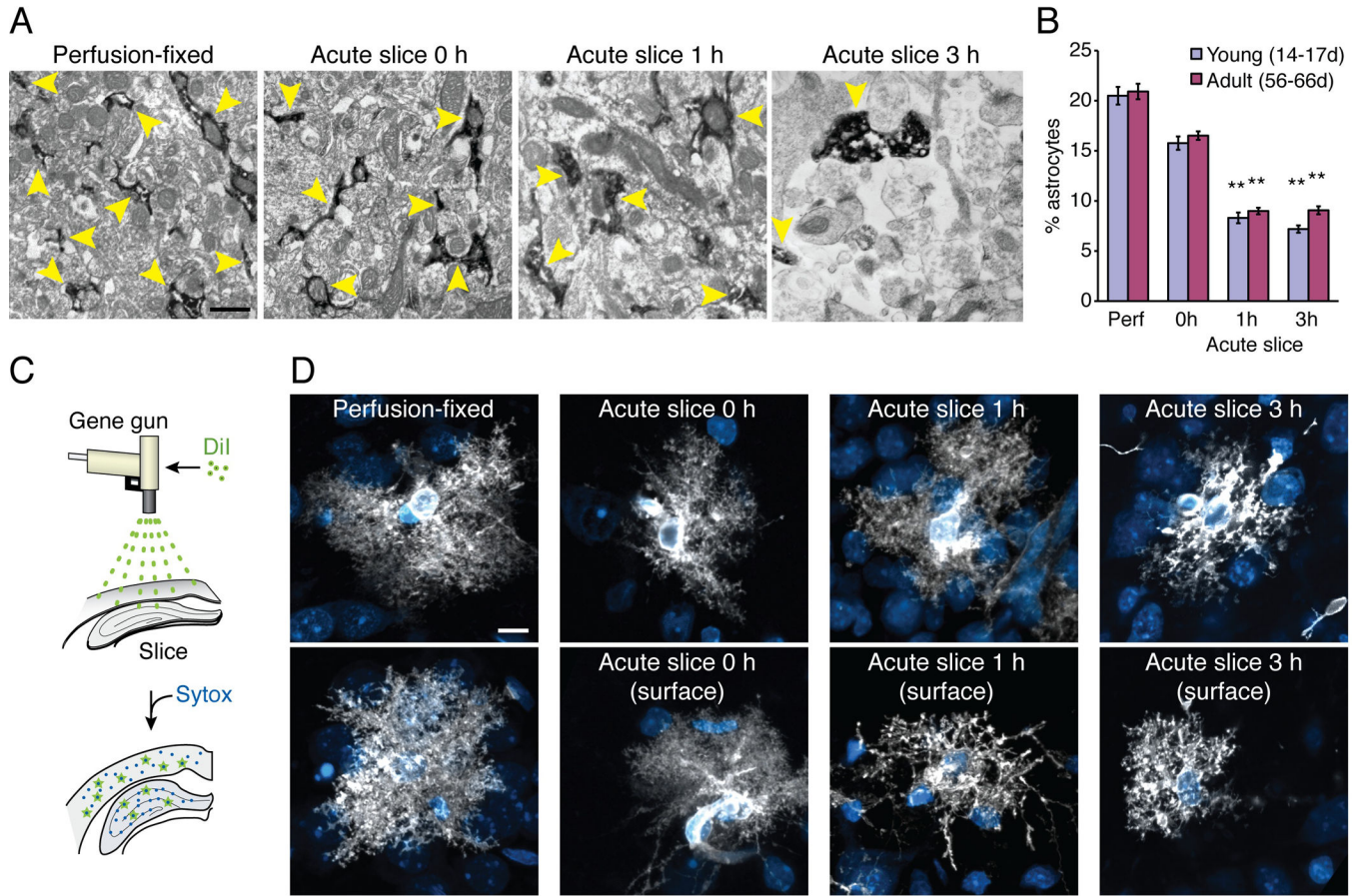
Fig. 5. Loss of fine astrocytic processes in acute hippocampal slices
ImmunoEM comparing fine astrocytic processes in perfusion- versus immersion-fixed acute hippocampal slices prepared from GFAP-GFP reporter mice. (**A**) Astrocytic processes (yellow arrowheads) were clearly identified in sections immunolabeled against GFP (dark in immunoEM), because GFP is a cytosolic protein present in even the finest protrusions. In perfusion-fixed animals, as well as in slices immersion-fixed immediately after vibratome cutting (0 h), astrocytic processes were irregular with the typical edgy protrusions. GFP-positive processes were rounded and often positioned in close proximity to areas free of cytosolic content (interstitial space), which were essentially absent in perfusion-fixed animals. Scale bar, 0.7 μm. (**B**) Comparison of the relative area of GFP$^+$ processes occupied in the total field in perfusion-fixed (Perf) versus immersion-fixed slices at 0, 1, and 3 h after vibratome cutting taken from young (14–17 days postnatal) and adult (56–66-day-old) animals (N=40 fields from 9 animals, Mean ± sem, **, $p<0.01$, Kruskal-Wallis test with Dunn's test against perfusion fix). (**C**) Schematic diagram of the procedure for diolistic labeling. Small gold particles coated with DiI were ballistically delivered to the slices. (**D**) The classical haze of fine astrocytic protrusions was evident in astrocytes in perfusion-fixed slices and in slices immersion fixed at 0 or 1 h after vibratome cutting. However, astrocytes with loss of fine processes were present at the surface of the slices immersion fixed at 1 and 3 h after preparation. Scale bar, 10 μm.
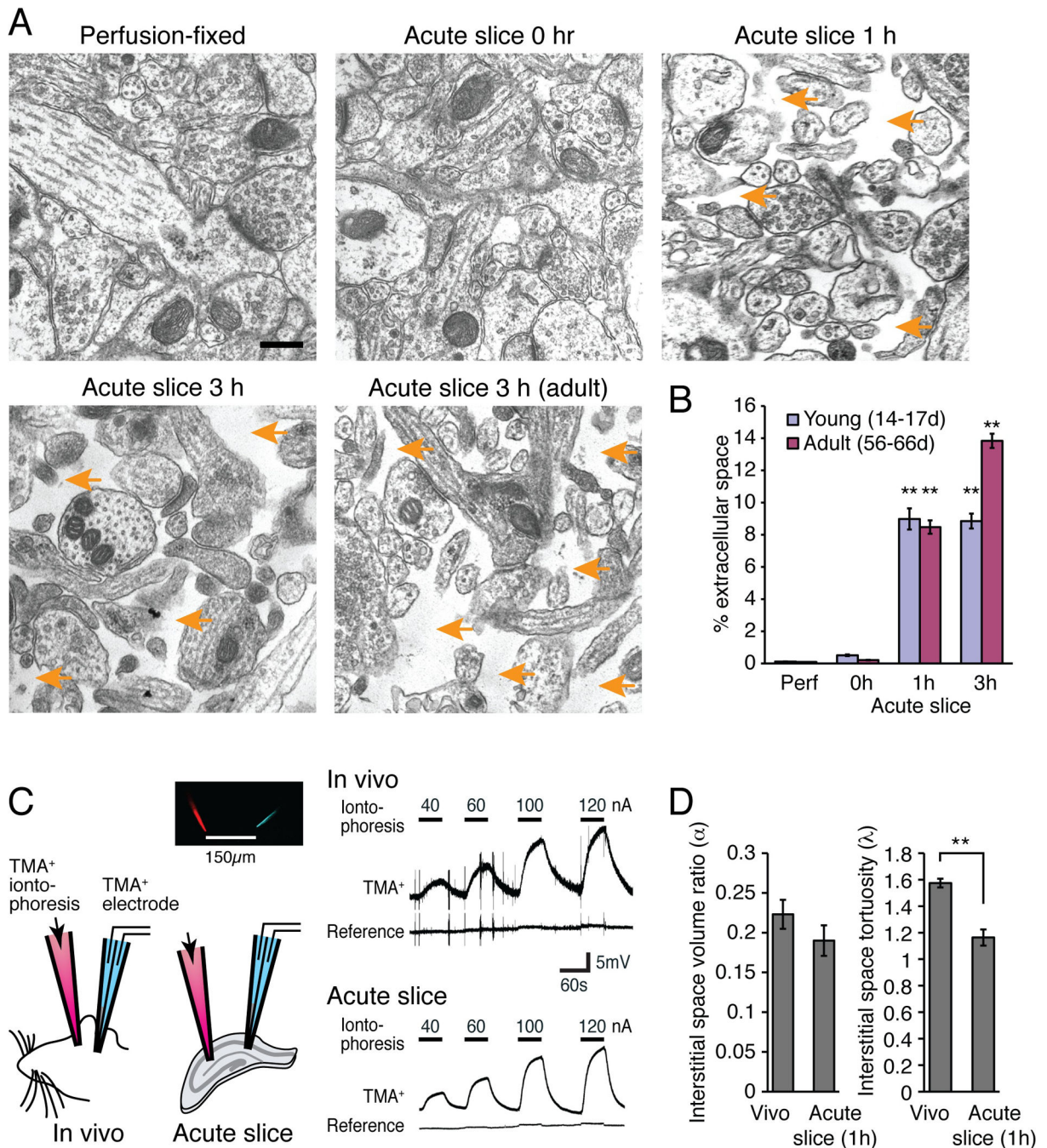
Fig. 6. Changes in the interstitial space volume and tortuosity in acute hippocampal slices
(**A**) Regular EM showed that the interstitial space (orange arrows) expanded during incubation of hippocampal slices in an oxygenated aCSF. Scale bar, 0.3 μm. (**B**) Comparison of the relative extracellular space in perfusion-fixed (Perf) versus immersion-fixed slices at 0, 1, and 3 h after vibratome cutting taken from young (14–17-day-old postnatal pups) and adult (56–66-day-old) animals (N=40 fields from 9–18 animals, Mean ± sem, **, p<0.01, Kruskal-Wallis test with Dunn's test against perfusion fix). (**C**) Real-time ionophoretic TMA$^+$ measurement of interstitial space in slices (1 h after preparation) and *in vivo* using a

double-barrel electrode comprised of TMA$^+$ sensitive and K$^+$ reference electrodes placed at 150 μm away from the TMA$^+$ iontophoresis. (**D**) Histograms showing the interstitial space volume fraction (α) and tortuosity (λ) of the extracellular space (N=7–12, Mean ± sem, **, p < 0.01, t tests).
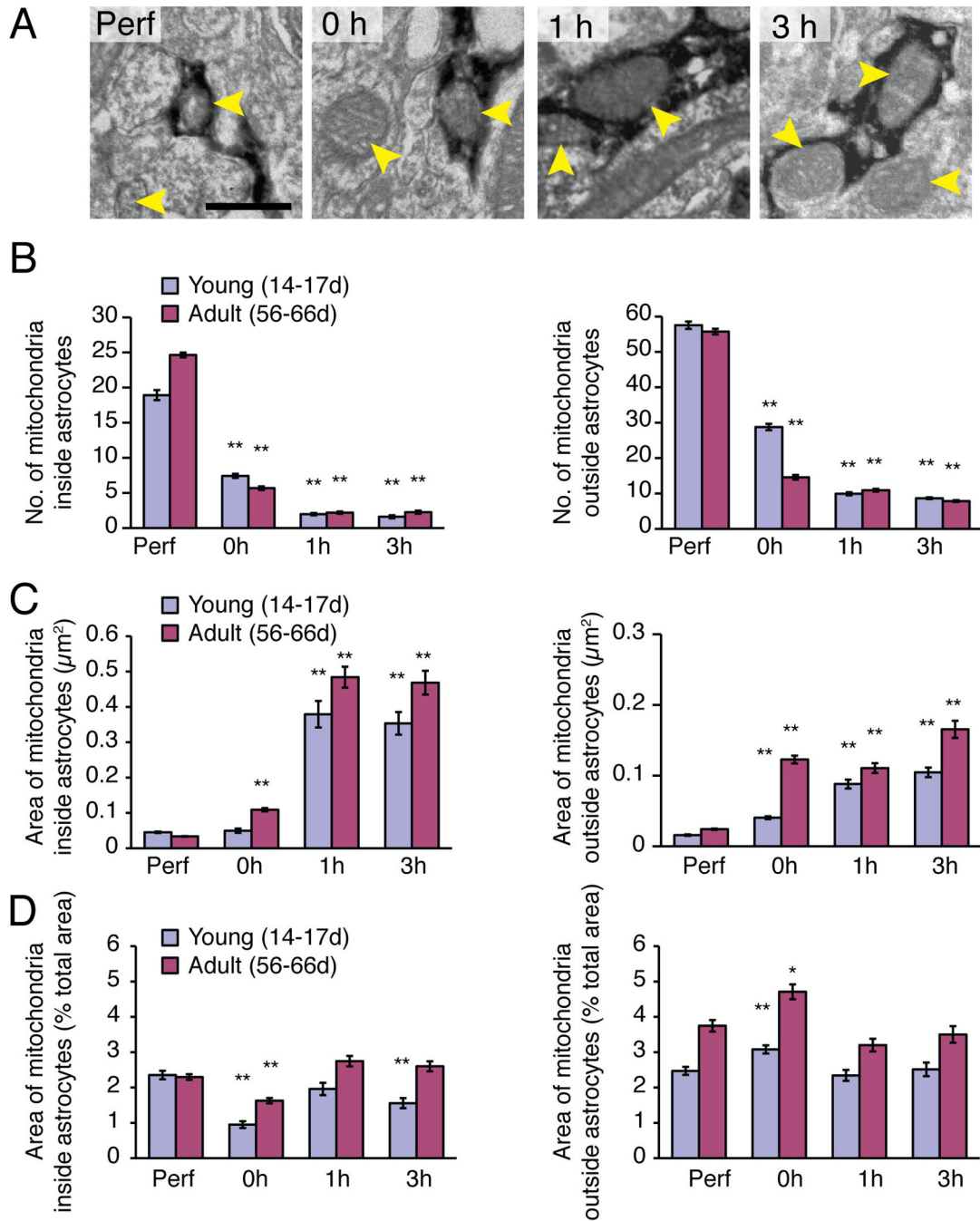
Fig. 7. The number and size of mitochondria undergo major changes upon slice preparation
A striking increase in the size of mitochondria was noted concurrent with a decrease in their
number in immersion-fixed hippocampal slices. (**A**) ImmunoEM of GFAP-GFP reporter
mice was used to identify mitochondria (yellow arrows) inside GFP[+] astrocytic processes
(stained dark) and unstained GFP[−] processes in perfusion- (Perf) and immersion-fixed slices
(0, 1, and 3h). Scale bar, 0.5 μm. (**B**) Histogram comparing the number of mitochondria in
perfusion-fixed (Perf) vs. immersion-fixed slices 0, 1, or 3 h after vibratome cutting taken
from young (14–17 days post natal) and adult (56–66 day old) animals (N=40 fields from 9

animals, Mean ± sem, **, p<0.01, Kruskal-Wallis test with Dunn's test against perfusion fix). (**C**) Comparison of the average cross-sectional area of mitochondria in perfusion-fixed versus slices immersion-fixed 0, 1, or 3 h after vibratome cutting (N=40 fields from 9 animals, Mean ± sem, **, p<0.01, Kruskal-Wallis test with Dunn's test against perfusion fix). (**D**) Calculation of the cross-sectional area of all mitochondria within GFP$^+$ astrocytic processes and GFP$^-$ processes from other cell types normalized to the total area of the field. The cross-sectional area of mitochondria remained relatively constant across all groups, suggesting that the loss of mitochondria combined with an increase in their average size reflected mitochondrial fusion (N=40 fields from 9 animals, Mean ± sem, *, p < 0.05, **, p<0.01, Kruskal-Wallis test with Dunn's test against perfusion fix).
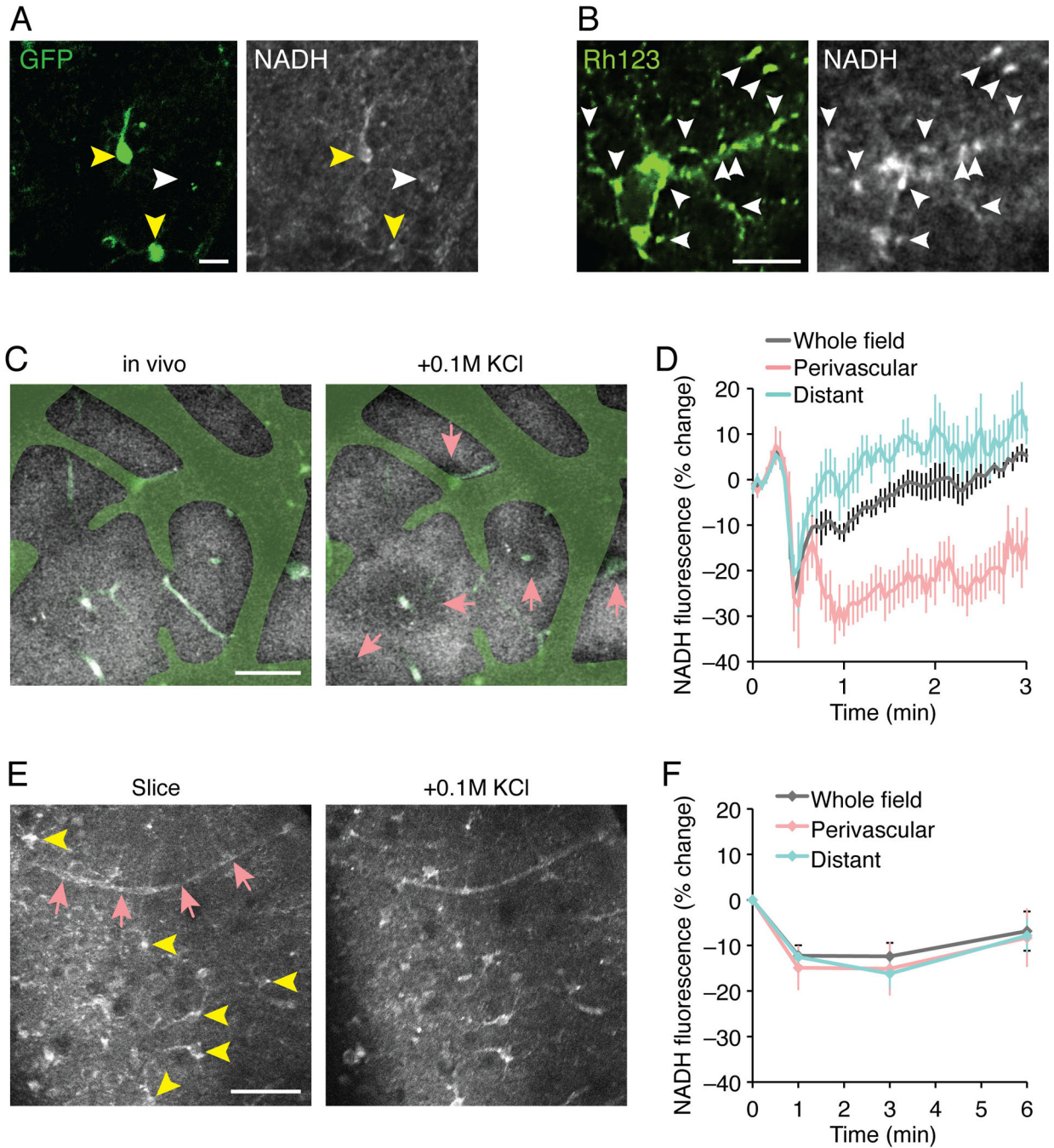
Fig. 8. Imaging of NADH concentration reveals marked regional differences in redox state after exposure to high K$^+$

(**A**) NADH fluorescence is higher in astrocytes in acute slices. Astrocytes identified by GLT-1-GFP (green, yellow arrowheads) are outlined more prominently in NADH fluorescence compared to other cell types (white arrowheads). Scale bar, 10 μm. (**B**) A high-magnification view of single astrocyte showed high NADH fluorescence co-localized with mitochondria identified by rhodamine 123 (Rh123, white arrowheads). Scale bar, 10 μm. (**C**) A low-magnification view of NADH fluorescence in intact cerebral cortex *in vivo* (60

μm deep) appeared relatively uniform. Faded green indicates the area where the NADH image was masked by the shadows of pial surface vasculature, and light greens indicate blood vessels inside the tissue visualized by systemic injection of FITC-dextran. After topical application of 0.1 M KCl, NADH fluorescence of tissue near penetrating blood vessels (pink arrows) decreased (more oxidized), while in the other regions NADH levels increased (more reduced). Scale bar, 50 μm. (**D**) A summary histogram of percent change of NADH fluorescence from the initial fluorescence at time 0, evoked by KCl in tissue near penetrating vessels (perivascular), distant from the penetrating vessels (distant), and whole tissue (N=5 animals, Mean ± sem). (**E**) In acutely isolated slices (1 h), NADH fluorescence prominently highlights cellular structures (yellow arrowheads) and vasculature (pink arrows). After topical application of 0.1 M KCl, NADH fluorescence showed overall decrease regardless of the position relative to the blood vessels. Scale bar, 50 μm. (**F**) A summary histogram of NADH fluorescence change by KCl in tissue near penetrating vessels (perivascular), distant from the penetrating vessels (distant), and whole tissue (N=5–8 slices, Mean ± sem).
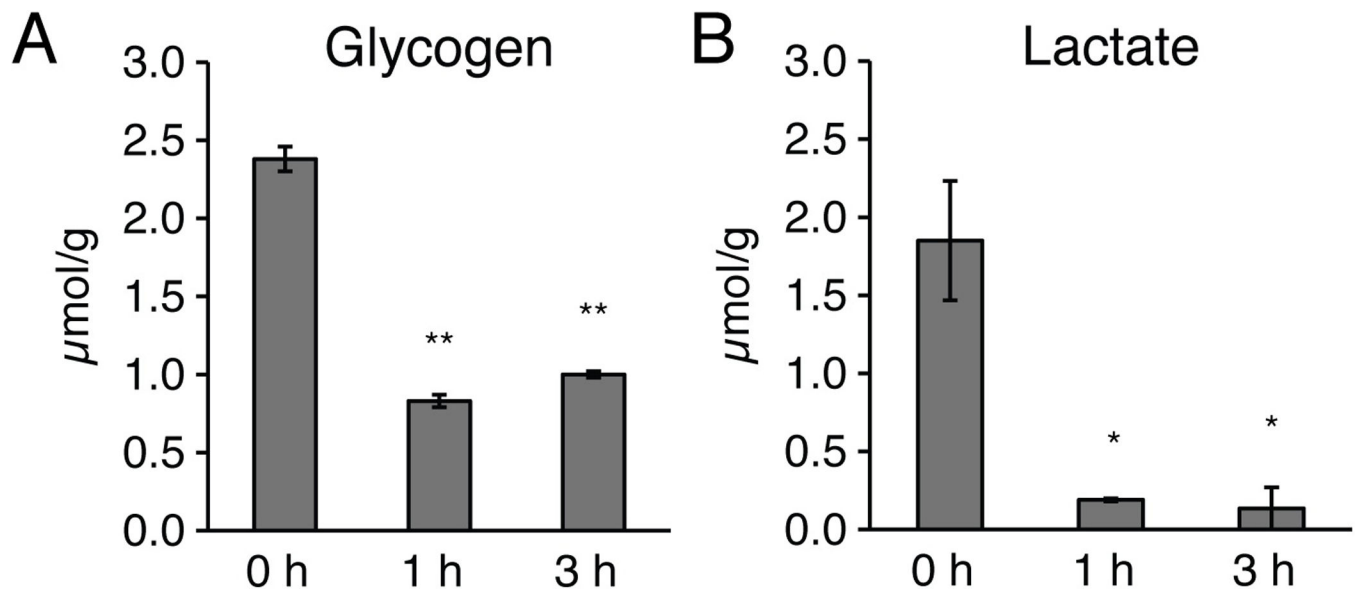
Fig. 9. Acute slices are depleted of glycogen for at least 3 h after cutting
(**A**) Quantification of glycogen and (**B**) lactate in acute hippocampal slices harvested at 0, 1, or 3 h after vibratome cutting (*, $p < 0.05$, **, $p < 0.01$, ANOVA with Tukey-Kramer tests).